Earth Surf. Dynam. Discuss., 2, 477–533, 2014
www.earth-surf-dynam-discuss.net/2/477/2014/
doi:10.5194/esurfd-2-477-2014

Earth Surface Dynamics Discussions
Open Access

Numerical modelling of Glacial Lake Outburst Floods using physically based dam-breach models

M. J. Westoby[1], J. Brasington[2], N. F. Glasser[3], M. J. Hambrey[1], J. M. Reynolds[3], and M. A. A. M. Hassan[4]

[1]Department of Geography and Earth Sciences, Aberystwyth University, UK
[2]School of Geography, Queen Mary, University of London, UK
[3]Reynolds International Ltd, Suite 2, Broncoed House, Broncoed Business Park, Mold, UK
[4]HR Wallingford Ltd, Howberry Park, Wallingford, Oxfordshire, UK

Received: 9 May 2014 – Accepted: 2 June 2014 – Published: 13 June 2014

Correspondence to: M. J. Westoby (mjwestoby@gmail.com)

Published by Copernicus Publications on behalf of the European Geosciences Union.

Abstract

The rapid development and instability of moraine-dammed proglacial lakes is increasing the potential for the occurrence of catastrophic Glacial Lake Outburst Floods (GLOFs) in high-mountain regions. Advanced, physically-based numerical dam-breach models represent an improvement over existing methods for the derivation of breach outflow hydrographs. However, significant uncertainty surrounds the initial parameterisation of such models, and remains largely unexplored. We use a unique combination of numerical dam-breach and two-dimensional hydrodynamic modelling, employed with a Generalised Likelihood Uncertainty Estimation (GLUE) framework to quantify the degree of equifinality in dam-breach model output for the reconstruction of the failure of Dig Tsho, Nepal. Monte Carlo analysis was used to sample the model parameter space, and morphological descriptors of the moraine breach were used to evaluate model performance. Equifinal breach morphologies were produced by parameter ensembles associated with differing breach initiation mechanisms, including overtopping waves and mechanical failure of the dam face. The material roughness coefficient was discovered to exert a dominant influence over model performance. Percentile breach hydrographs derived from cumulative distribution function hydrograph data under- or overestimated total hydrograph volume and were deemed to be inappropriate for input to hydrodynamic modelling. Our results support the use of a Total Variation Diminishing solver for outburst flood modelling, which was found to be largely free of numerical instability and flow oscillation. Routing of scenario-specific optimal breach hydrographs revealed prominent differences in the timing and extent of inundation. A GLUE-based method for constructing likelihood-weighted maps of GLOF inundation extent, flow depth, and hazard is presented, and represents an effective tool for communicating uncertainty and equifinality in GLOF hazard assessment. However, future research should focus on the utility of the approach for predictive, as opposed to reconstructive GLOF modelling.

ESURFD

2, 477–533, 2014

1 Introduction

Glacier recession has been observed on a global scale as a result of recent climatic change (Oerlemans, 1994; Kaser et al., 2006; Zemp et al., 2009; Bolch et al., 2011, 2012). The exposure of terminal and lateral (combined: "latero-terminal") moraine complexes is becoming increasingly commonplace as a result of glacier recession, particularly in high-mountain regions. Latero-terminal moraines reflect the historical maximum extent of a given glacier, and are typically composed of poorly-consolidated glacial material.

Moraine-dammed lakes form through one of two mechanisms, namely: recession of the glacier terminus and ponding of water in the proglacial moraine basin (Frey et al., 2010), or via the coalescence and expansion of supraglacial ponds on heavily debris-covered glaciers (Reynolds, 1998, 2000; Richardson and Reynolds, 2000; Benn et al., 2001, 2012; Thompson et al., 2012). Following expansion, such lakes are capable of impounding volumes of water in excess of 10^6–10^7 m^3 (Lliboutry, 1977a; Vuichard and Zimmerman, 1987; Watanabe et al., 1995; Sakai et al., 2000; Janský et al., 2009).

Moraine breaching may result in the generation of a Glacial Lake Outburst Flood (GLOF) (Lliboutry, 1977a; Vuichard and Zimmerman, 1987; Clague and Evans, 2000; Kershaw et al., 2005; Harrison et al., 2006; Osti and Egashira, 2009; Worni et al., 2012; Westoby et al., 2014). These sudden-onset outburst floods represent high-magnitude, low-frequency catastrophic phenomena that have enormous potential for geomorphological reworking of channel and floodplain environments (Cenderelli and Wohl, 2003) including the destruction of land, buildings and infrastructure in, or adjacent to the flood path, and can result in human fatalities (Vuichard and Zimmerman, 1987; Lliboutry et al., 1977a; Watanabe and Rothacher, 1996). Of the various glacial hazards (Richardson and Reynolds, 2000; Kääb et al., 2005; Quincey et al., 2005, 2007), GLOFs have the most far-reaching impacts, with destruction often reported tens or hundreds of kilometres from their source (Vuichard and Zimmerman, 1987; Clague and Evans, 2000; Richardson and Reynolds, 2000).

ESURFD
2, 477–533, 2014

2 Study site

The Dig Tsho moraine-dammed lake complex is located at the head of the Langmoche valley in the western sector of Sagarmatha (Mt. Everest) National Park in the Khumbu Himal (Solukhumbu District), Nepal (Fig. 1; 27°52′23.89″ N, 86°35′14.91″ E). A relict moraine-dammed lake, oriented west-east, is impounded by a latero-terminal moraine complex to the north and east. The basin is bounded by a near-vertical bedrock face to the south. The parent Langmoche Glacier has receded significantly since its Neoglacial maximum terminus position and is now confined to the upper north-east faces of Tangi Ragi Tau (6940 m).

The moraine possesses steep (25–30°) faces on all ice-distal sides and on ice-proximal sides along the northern lateral moraine. In contrast, proximal faces of the terminal moraine are generally shallower, although ice-proximal faces are more topographically complex than their distal counterparts. The moraine is composed of sandy boulder-gravel, and includes rare large (> 10 m diameter) boulders. A sizeable (200 m wide, 400 m long, 60 m deep) breach dissects the northern sector of the terminal moraine (Fig. 1; Vuichard and Zimmerman, 1987; Westoby et al., 2012).

On 4 August 1985 an ice avalanche from the receding Langmoche Glacier traversed the steep (∼ 30°) avalanche and debris cone which terminates in the moraine-dammed lake and triggered a displacement wave that was transmitted along its length. This initial wave is believed to have overtopped the moraine dam, thereby initiating its failure. Although not observed first-hand, full breach formation was estimated to have taken 4–6 h (Vuichard and Zimmerman, 1987).

The geomorphological effects of the Dig Tsho GLOF have been well documented (Vuichard and Zimmerman, 1986, 1987; Cenderelli and Wohl, 2001, 2003). A newly-completed hydro-electric power installation adjacent to the village of Thamo was completely destroyed (∼ 11.5 km from source). All trekking bridges for a distance of > 30 km were destroyed and up to 5 people are reported to have been killed (Galay, 1985).

ESURFD
2, 477–533, 2014

Existing observational data for the site include first-hand descriptions of the condition of the glacial lake prior to, and immediately following moraine dam failure in 1985, as well as a description of the pre-GLOF nature of the valley floor sedimentology immediately downstream (Vuichard and Zimmerman, 1987). Existing estimates state the mass of material removed from the breach as being 9×10^5 m^3, and the drained volume of the moraine basin as being 5×10^6 m^3. It is envisaged that the vast majority of the dam material eroded during breach development was deposited within 2 km of the moraine. Field investigation and photogrammetric reconstruction of the moraine by Westoby et al. (2012) has revealed the volume of the contemporary breach (surveyed in 2010) to be approximately 5.8×10^5 m^3, and the volume of water released by the 1985 GLOF to be $\sim 7.3 \times 10^6$ m^3. Sedimentological (D_{50}) sampling of matrix material exposed in the breach sidewalls was undertaken during field investigation, and was used to aid dam-breach model parameterisation.

3 Quantifying equifinality and uncertainty in a numerical dam-breach model

3.1 Motivation for this study

Numerous sources of uncertainty are associated with the parameterisation of contemporary numerical dam-breach and hydrodynamic models for reconstructive or predictive GLOF simulation (Westoby et al., 2014). Few studies have sought to explore the sensitivity of dam-breach models to parametric uncertainty (e.g. Wang et al., 2012; Worni et al., 2012) and the extent and significance of model equifinality for GLOF inundation and hazard mapping. This article seeks to address this increasingly conspicuous research gap through the development and demonstration of a unifying framework for cascading uncertainty and equifinality in the GLOF model chain through the reconstruction of a historical GLOF in the Nepalese Himalaya.

ESURFD
2, 477–533, 2014

3.2 The role of uncertainty and equifinality in dam-breach modelling

Equifinality is where identical or similar end states in an open system are achieved from many different combinations of input parameters, initial conditions, and model structures (e.g. Beven and Binley, 1992; Beven and Freer, 2001; Beven, 2005). In geomorphological investigation, equifinality explains how a single landform or landform assemblage may have formed through a range of differing, but equally plausible process combinations (e.g. Nicholas and Quine, 2010; Stokes et al., 2011). Equifinality has its origins in systems theory (von Bertalanffy, 1968), and has been recognised and quantified in a range of geoscience applications (e.g. Beven and Binley, 1992; Kuczera and Parent, 1998; Lamb et al., 1998; Romanowicz and Beven, 1998; Beven and Freer, 2001; Blazkova and Beven, 2004; Hunter et al., 2005; Cameron, 2007; Hassan et al., 2008; Rojas et al., 2008; Vasquez et al., 2009; Vrugt et al., 2009; Franz and Hogue, 2011).

Uncertainty abounds at both the dam-breach and hydrodynamic, flood-routing stages of the GLOF model chain (Westoby et al., 2014). In the case of the former, appreciable uncertainty surrounds the establishment of initial conditions (e.g. dam geometry, reservoir hypsometry), dam material parameterisation (e.g. grain-size distribution curves, material porosity, density, cohesion, roughness coefficients, internal angle of friction) and the establishment of computational constraints (e.g. model time step and grid discretisation).

Variability in hydrodynamic model output may be attributed to model dimensionality (e.g. Alho and Aaltonen, 2008; Bohorquez and Darby, 2008), grid discretisation and quality (e.g. Sanders, 2007; Huggel et al., 2008) the spacing of cross-sections used to represent floodplain geometry in 1-D hydrodynamic models (e.g. Castellarin et al., 2009), as well as uncertainty surrounding the parameterisation of in-channel and floodplain roughness coefficients (Wohl, 1998; Hall et al., 2005; Pappenberger et al., 2005), boundary condition data (e.g. Pappenberger et al., 2006) and stage–discharge relationships (e.g. Di Baldassarre and Claps, 2011). Recent studies have undertaken various

ESURFD
2, 477–533, 2014

forms of sensitivity analyses and uncertainty estimation to quantify the effects of uncertainty on numerical dam-breach model output (e.g. IMPACT, 2004; Xin et al., 2008; Dewals et al., 2011; Zhong et al., 2011; Worni et al., 2012). However, to date issues of equifinality remain largely unexplored.

4 Method

We approach the problem of developing a framework for embracing and propagating parameter uncertainty through the GLOF model chain by using a sequence of methods. In the order that they are encountered in our modelling chain, these include: (i) digital terrain modelling using terrestrial photogrammetry to reconstruct pre-existing moraine and floodplain topography and extraction of glacial lake bathymetry and dam geometry data, (ii) parameterisation of a numerical dam-breach model using material properties obtained through field investigation and from published literature, (iii) stochastic dam-breach model parameter sampling and model execution to obtain a series of scenario-specific dam-breach hydrographs, (iv) the application of Bayesian statistics, based on geometric descriptors of observed, post-GLOF breach topography, to evaluate the performance of individual dam-breach simulations, and, (v) the application of a two-dimensional hydrodynamic solver to model the downstream propagation of retained GLOF hydrographs and provide inundation extent, flow velocity, and flow depth data for use as input to probabilistic GLOF hazard mapping. The following sections describe each method in detail.

4.1 Topographic data acquisition

Structure-from-Motion (SfM) photogrammetry, combined with Multi-View Stereo (MVS) methods (James and Robson, 2012; Westoby et al., 2012; Fonstad et al., 2013; Javernick et al., 2014) was used to reconstruct floodplain topography for a distance of ~ 2 km downstream of Dig Tsho. The SfM method requires the acquisition of photosets with

ESURFD
2, 477–533, 2014

a high degree of image overlap and feature coverage from a range of perspectives, followed by the application of feature extraction (e.g. Lowe, 2004) and bundle adjustment algorithms (e.g. Snavely, 2008; Snavely et al., 2008) for the sparse and dense reconstruction of 3-D scene geometry.

Reconstruction of moraine topography using SfM-MVS methods is described in detail in Westoby et al. (2012). Here, we use their SfM-derived terrain model of the Dig Tsho moraine to extract metric data describing to moraine geometry and lake basin hypsometry (Fig. 2) for the establishment of initial conditions for numerical dam-breach modelling.

To reconstruct post-GLOF valley-floor topography, two photosets, numbering 226 and 303 photographs for south- and north-facing perspectives respectively, were acquired from successive elevated positions on the valley flanks using a Panasonic DMC-G10 (12 MP) digital camera with automatic focusing and exposure settings enabled. The freely-available software bundle SFMToolkit3 (Astre, 2010) was used to process the input images using feature extraction (Lowe, 2004) and sparse and dense SfM-MVS reconstruction algorithms. Following manual outlier removal and editing, final dense point clouds numbered 4.8×10^6 and 1.3×10^6 points for north- and south-facing photosets respectively. Data transformation was achieved through the identification of clearly-identifiable boulders from kite aerial photography and an existing SfM-derived Digital Terrain Model (DTM) of the easternmost sector of the floodplain domain, as well as boulders visible in the georeferenced DTM of the moraine dam. Averaged georegistration residual errors for both dense point clouds were 1.37 m, 0.30 m and 0.06 m for *xyz* dimensions respectively.

Georeferenced point cloud data were merged and decimated to improve data handling whilst preserving sub-grid statistics using the C++/Python-based Topographic Point-Cloud Analysis Toolkit (Brasington et al., 2012; Rychkov et al., 2012). A bare-earth DTM at 8 m spatial resolution was extracted for hydrodynamic GLOF routing. Sensitivity analyses have previously revealed this particular grid discretisation to produce time-varying inundation extents and wetting-front travel times of comparable

ESURFD
2, 477–533, 2014

(relative) accuracies to those produced using finer grid resolutions, and of higher accuracy than coarser grids (Westoby et al., 2014).

4.2 Numerical dam-breach modelling using HR BREACH

HR BREACH is a physically-based, numerical dam-breach model that predicts the growth of a dam breach arising from the overtopping of non-cohesive and cohesive embankment materials, as well as via piping mechanisms (Morris et al., 2008; Westoby, 2013; Westoby et al., 2014). In contrast with analytical- or parametric-type models, HR BREACH combines a range of hydraulic, sediment erosion and discrete embankment stability analyses to facilitate the "free" formation of breach geometry and generation of the outflow hydrograph (Morris et al., 2008). Crucially, it has not been directly calibrated to data from one or more specific events.

HR BREACH handles breach enlargement through the interaction of two mechanisms, namely: (i) continuous erosion of submerged sediment through the application of equilibrium sediment transport equations or erosion-depth equations, and, (ii) discrete mass failures due to side-slope instability (Mohamed et al., 2002). Erosion-depth equations are deemed to be highly appropriate for simulating dam breaching as they are deemed to be more physically representative of the hydraulic and sediment transport processes in operation during breach development. We use the erosion-depth equation for non-cohesive embankments, as forwarded by Chen and Anderson (1986):

$$\varepsilon_r = K_d(\tau_e - \tau_c)^a \quad (1)$$

where ε_r is the detachment rate per unit area (e.g. $m^3\,s^{-1}\,m^2$), τ_e the flow shear stress (kN) at the breach boundary, τ_c is the critical shear stress required to initiate particle detachment (kN), and K_d and a are dimensionless coefficients based on the sediment properties. Bending (tensional) failure is represented by a moment of force, M_o:

$$M_o = We + W_s e_s + W_u e_u + H_2 e_2 - H_1 e_1 \quad (2)$$

ESURFD
2, 477–533, 2014

where W is the weight of a dry block of soil, W_s is the weight of a saturated block of soil, W_u is the weight of a submerged block of soil, H_1 is the hydrostatic pressure force in the breach channel, H_2 is the hydrostatic pressure force inside the dam structure, e, e_s and e_u are weight force eccentricities, e_1 and e_2 are hydrostatic pressure force eccentricities (Hassan and Morris, 2012). The occurrence of shear-type failure is evaluated through the analysis of Factor of Safety (FoS) values using the following equation:

$$\mathrm{FoS} = \frac{cL + H_1 \tan\Phi}{W + W_s + W_u + H_2 \tan\Phi} \quad (3)$$

where c is soil cohesion, L is the length of the failure plane and Φ is the soil angle of friction.

Subaerial, steady-state breach flow is simulated using a one-dimensional flow model (Mohamed et al., 2002; Morris et al., 2008). This method combines a weir discharge equation and a simplified version of the Saint Venant equations (de St-Venant, 1871) to simulate breach flow, and flow descending the distal face of the dam, respectively. HR BREACH is capable of using variable weir discharge coefficients, which are automatically updated, based on the changing profile of the dam crest (Hassan and Morris, 2012) and is intended to compensate for the significant flow complexity which arises during breach development.

4.3 Generalised Likelihood Uncertainty Estimation (GLUE)

For event-specific flood reconstruction, systematic calibration of input parameters to produce best-fit, or optimal flood conditions is often practiced (e.g. Kidson et al., 2006; Cao and Carling, 2002). Model calibration typically comprises the adjustment of individual or multiple model parameters to provide a best-fit solution to an observed dataset (e.g. Refsgaard, 1997; Beven and Freer, 2001; Hunter et al., 2005; Westerberg et al., 2011) and may serve to inform their choice for hypothetical future events (e.g. Horritt and Bates, 2002).

ESURFD
2, 477–533, 2014

Where there is insufficient quantitative or qualitative information pertaining to the model parameterisation or simulation constraints, any combination of model input that reproduces the observed outcome, within acceptable limits, must be considered equally likely as a simulator of the system under investigation (Beven and Binley, 1992). This is the underlying principle of the Generalised Likelihood Uncertainty Estimation (GLUE) method (Beven and Binley, 1992; Beven, 2005). The following sections describe its application to quantifying equifinality in moraine-dam failure reconstruction using HR BREACH.

4.3.1 Parameter choice, prior distributions, and stochastic sampling

The first step in the GLUE workflow is to establish the parameters for inclusion and their respective ranges. In the absence of any prior information regarding parameter and range choice, all available input parameters and their entire simulation range should be included. In practice, complete uncertainty regarding parameter and range choice is unlikely, since a combination of initial sensitivity analyses, modelling guidelines, as well as basic intuition and reasoning can typically be used to assist in constraining their choice (Beven and Binley, 1992). The parameters and their ranges used in this study (including computational settings) are displayed in Table 1.

Information regarding initial, or a priori, parameter distributions is also required, reflecting the modeller's prior knowledge of the parameter space (Beven and Binley, 1992). In the absence of any information pertaining to a priori parameter probability distributions at Dig Tsho, uniform distributions were used for stochastic sampling of all available parameter spaces.

Although a range of stochastic sampling methods are available for use in the GLUE workflow (e.g. Metropolis, 1987; Iman and Helton, 2006), perhaps the most widely used approach is Monte Carlo analysis (e.g. Beven and Binley, 1992; Kuczera and Parent, 1998; Aronica et al., 1998, 2002; Blazkova and Beven, 2004). Using the Monte Carlo method, values from individual parameter spaces are sampled randomly, thereby eliminating any subjectivity which might be introduced at this stage. The method is fully

ESURFD
2, 477–533, 2014

capable of accounting for predefined probability distribution data, making it a simple yet effective tool for rapidly generating the random parameter ensembles required for model input. However, with a poorly-defined prior distribution, or a small number of model simulations, point clustering in specific regions of the parameter space may occur. Clustering can be easily avoided by undertaking a straightforward investigation into patterns of histogram convergence of an output variable (or variables), whereby the minimum number of simulations required for the production of an acceptable level of convergence is established. In our study, continued histogram convergence became minimal after the execution of 1000 model runs. This number of simulations was therefore deemed acceptable for stochastic sampling.

4.3.2 Likelihood measures and functions

Model evaluation is achieved through quantification of how well a parameter ensemble performs at reproducing a series of observable system state variables, or likelihood measures. Parameter ensembles that are unable to do so are deemed to be non-behavioural and are assigned a likelihood score of zero. In contrast, ensembles that reproduce these variables within acceptable limits are deemed to be behavioural and accepted for further analysis. It is not uncommon for all ensembles to be rejected (e.g. Parkin et al., 1996; Freer et al., 2002), thereby suggesting that it is in fact the model structure that is incapable of reproducing the observed data, instead of individual parameter combinations (Beven and Binley, 1992). Such a situation may be overcome by widening the limits of acceptability, but at the potential cost of decreasing confidence in any newly-accepted ensembles (Beven and Binley, 1992).

Behavioural ensembles were assigned positive likelihood values in the range 0–1, where 1 represents an ensemble that is capable of perfectly replicating the observed data. Likelihood functions are specific to each likelihood measure used for model evaluation. Three likelihood measures were used to evaluate HR BREACH model performance: (i) final upstream breach depth (LH1), (ii) the residual sum of squared errors of the final longitudinal elevation profile of the breach (LH2), and, (iii) the location of the

ESURFD
2, 477–533, 2014

critical flow constriction (LH3; Fig. 3). These morphological variables are directly quantifiable through the comparison of final modelled breach geometry with that extracted from the SfM-DTM of the breached moraine-dam.

An observed breach depth of 16 ± 2 m was used. The error range was designed to account for observed SfM model georegistration errors, which may have resulted in elevation of the lake exit being under- or overestimated, as well as any post-GLOF lake lowering or seasonal variations in lake level, which remain unquantified. A triangular likelihood function was used, with an observed breach depth of 16 m and upper and lower limits defined as 14 m and 18 m respectively.

The second likelihood measure took the form of a direct comparison between observed (post-GLOF) and modelled elevation profiles of the breach thalweg. This measure represents an effective, distributed method of quantifying the performance of HR BREACH in producing post-GLOF thalweg elevation profiles that mirror, or significantly differ from that observed in the field. Thalweg elevation data were directly extracted from the SfM-DTM (Fig. 12a, Westoby et al., 2012). The residual sum of squares (RSS) method was used to quantify the deviation between the observed and modelled data:

$$\mathrm{RSS} = \sum_{i=1}^{n} (Z_{\mathrm{obs}} - Z_{\mathrm{pred.}})^2 \quad (4)$$

where Z_{obs} is the observed elevation (m) of the breach thalweg and $Z_{\mathrm{pred.}}$ is the elevation of the modelled thalweg. For the attribution of a scaled likelihood value, an RSS of 0 corresponded to a likelihood score of 1, whilst the lowest RSS for all scenarios (169 221; dimensionless) was used to represent the lower, non-behavioural limit. A simple linear likelihood function was applied.

Choice of an observed value for the location of the critical flow constriction was complicated by the asymmetry of the observed breach planform, whereby flow constrictions on either side of the breach are offset by a distance of approximately 40 m. Precisely why this asymmetry exists is inexplicable in the absence of any detailed observations of breach development, but is most likely a function of complex flow hydraulics and

ESURFD
2, 477–533, 2014

patterns of erosion of the moraine during breach expansion. Use of a trapezoidal likelihood function would have been possible, whereby any modelled values that fell between the observed constriction "offset zone" would be assigned a likelihood of 1. However, such an approach was deemed inappropriate, because it would render a significant proportion of parameter ensembles as absolutely behavioural. Instead, a triangular likelihood function was used. The mid-point of the observed offset was used as the central, observed value, and a range of ±40 m was applied to encompass observed asymmetry in flow constriction location.

4.3.3 Likelihood updating

Where multiple likelihood measures are used, it is necessary to arrive at a final, global likelihood value for each behavioural parameter ensemble. Bayesian updating represents a statistically robust method for combining multiple likelihood values, as it is able to account for the influence of prior likelihood values on the generation of updated values as more data become available. Implementation of the Bayesian updating approach used here is summarised as (modified from Lamb et al., 1998):

$$L(\Theta_i|Y_{1,2}) = \frac{L(\Theta_i|Y_1)L(\Theta_i|Y_2)}{C} \quad (5)$$

with:

$$C = (L(\Theta_i|Y_1)L(\Theta_i|Y_2)) + (L(\Theta_i|Y_1^i)L(\Theta_i|Y_2^i)) \quad (6)$$

where $L(\Theta_i|Y_{1,2})$ is the conditional posterior likelihood for a parameter ensemble, Θ_i, conditioned on two sets of observations, Y_1 and Y_2, $L(\Theta_i|Y_1)$. is the likelihood of Θ_i conditioned on an initial set of observations (Y_1), $L(\Theta_i|Y_2)$ becomes the likelihood conditioned on a second, or additional set of observations (Y_2), and C is a conditional operator, or scaling constant, to ensure the cumulative posterior likelihood equals unity (Lamb et al., 1998; Hunter et al., 2005). The 'i' superscript refers to the inverse of the relevant conditional likelihood values.

ESURFD
2, 477–533, 2014

4.3.4 Cumulative Distribution Function generation

Final likelihood values associated with each behavioural parameter ensemble reflect the confidence of the modeller in the ability of each ensemble to reproduce an observed dataset. Considering the cumulative distribution of these global likelihood values as a probabilistic function facilitates an assessment of the degree of uncertainty associated with the behavioural predictions (Beven and Binley, 1992). These data are referred to as Cumulative Distribution Functions (CDFs).

Measure-specific likelihood values for each behavioural ensemble are were re-scaled to sum to unity. The final measure can be treated as a surrogate for true probability, but cannot be used for subsequent statistical inference (Hunter et al., 2005). Weighted and re-scaled ensembles are ranked and plotted as a CDF curve (Fig. 4), from which cumulative prediction limit data can be extracted (Beven and Binley, 1992). The generation of weighted CDFs is unique to the GLUE approach and represents a multivariate, additive method that accounts for ensemble performance.

4.4 Model perturbations

A control scenario was formulated, in which breach formation was initiated through down-cutting of an existing spillway as a result of flow produced by the pressure head associated with our specified initial lake level (which mirrored the modelled dam crest elevation of 4356 m a.s.l.) The modelled spiillway measured 0.5 m wide and 0.5 m deep and extended from the upstream end of the moraine crest, to the dam toe. We note that in the absence of detailed observations of the spillway prior to dam failure (Vuichard and Zimmerman, 1987), these dimensions are hypothetical and do not necessarily replicate the precise spillway conditions prior to dam failure in 1985.

In addition to a control scenario (*DT_control*), two styles of system perturbation scenario were introduced to the dam-breach models to explore and quantify the impact of system-scale perturbations on model output. These perturbations were: (i) the introduction of overtopping waves of varying magnitude, and, (ii) the instantaneous removal

ESURFD
2, 477–533, 2014

of material from the downstream face of the dam immediately prior to breach development

4.4.1 Overtopping waves

The failure of Dig Tsho has been attributed to the overtopping of the terminal moraine by waves produced by an ice avalanche from the receding Langmoche Glacier (Vuichard and Zimmerman, 1987). Presently, most numerical dam-breach models, including HR BREACH, are unable to explicitly simulate the dynamic effects of avalanche-lake interactions. This necessitated an inventive, yet relatively simple approach to reconstructing overtopping behaviour in HR BREACH. Instead of simulating the passage of a series of gradually attenuating displacement or seiche waves and dynamic interaction with the dam structure, a solution was devised which involved the rapid increase and subsequent decrease of the lake water surface elevation, which prompted short-lived overtopping of the dam structure at predefined intervals. Temporary increases in lake level were achieved through systematic variation of reservoir inflow to introduce maximum overtopping discharges of $4659\,m^3\,s^{-1}$, $3171\,m^3\,s^{-1}$ and $1809\,m^3\,s^{-1}$, representing initial volumes of the triggering avalanche of $2.0 \times 10^5\,m^3$, $1.5 \times 10^5\,m^3$ and $1.0 \times 10^5\,m^3$, respectively (and reflecting the estimated volumetric range provided by Vuichard and Zimmerman, 1987), with each followed by successive waves of exponentially-decaying magnitude. Overtopping wave scenarios were named *DT_overtop_min*, *DT_overtop_mid*, and *DT_overtop_max*, respectively.

4.4.2 Instantaneous mass removal

Richardson and Reynolds (2000) suggest that the initial failure of a moraine dam may be "explosive" in nature. This explosive force is reflected by the mass of individual clasts, which can exceed > 100 t (Richardson and Reynolds, 2000). Osti et al. (2011) documented the destabilisation and landsliding of morainic material from the Tam Pokhari moraine dam, Nepal, as a result of seismic activity and excessive rainfall, which

ESURFD
2, 477–533, 2014

caused oversaturation and subsequent partial failure of a section of the proximal dam structure, which contributed to its eventual failure and the generation of a GLOF.

HR BREACH requires that the user specify an initial breach spillway in the dam crest and downstream face of the dam. To simulate the instantaneous removal of material from the dam structure, three mass-removal scenarios were developed. The default spillway dimensions used in the control and overtopping experiments were 0.5 m wide and 0.5 m deep. Perturbed spillways cross-sectional dimensions were 1 m^2, 3 m^2 and 5 m^2, representing respective total removal volumes of 159 m^3, 1435 m^3, and 3987 m^3 of material and named *DT_instant_1*, *DT_instant_3* and *DT_instant_5*, respectively.

4.5 Two-dimensional hydrodynamic modelling

4.5.1 ISIS 2-D

The shallow-water flow model ISIS 2-D (Halcrow, 2012) was used to simulate GLOF propagation. The model includes Alternating Direction Implicit (ADI) and MacCormack-Total Variation Diminishing (TVD) two-dimensional solvers for hydrodynamic simulation. The ADI scheme solves the shallow-water equations (SWEs) over a regular grid of square cells. Water depth is calculated at cell centres, and flow discharges at cell boundaries. The SWEs are solved by sub-dividing the computation into x- and y-dimensions. Water depth (m) and discharge (q_x; per unit width) are solved in the x-dimension in the first half of the time step. Water depth and discharge (q_y) in the y-dimension are solved in the latter half of the time step. Other variables are represented explicitly for each stage. Since water depths are calculated at the cell centre, depths at cell boundaries are interpolated. Different interpolation methods are used, depending on water depth (Liang et al., 2006). Treatment of the friction term is also depth-dependent, such that below a user-defined threshold, a semi-implicit scheme is used to improve model stability with decreasing flow depth (Halcrow, 2012). The ADI scheme provides accurate solutions for flows where spatial variations are smooth. Sudden changes in water elevation and flow velocity may give rise to numerical oscillations,

ESURFD
2, 477–533, 2014

making it largely unsuitable for the simulation of transcritical flow regimes (Liang et al., 2006).

In contrast, the MacCormack-TVD scheme uses predictor and corrector steps to compute depth and discharge for successive time steps. A TVD term, Var(h), is added at the corrector step to supress numerical oscillations near sharp gradients, making it highly suited for the simulations of rapidly evolving, transcritical and supercritical flows (Liang et al., 2006), including sudden-onset floods arising from dam-breach (Liang et al., 2007; Liao et al., 2007). Var(h) is calculated as:

$$\mathrm{Var}(h) = \int \left| \frac{\delta h}{\delta x} \right| \mathrm{d}x \tag{7}$$

A far smaller time step is required to achieve numerical stability, resulting in extended model run times (Halcrow, 2012).

5 Results

5.1 Hydrodynamic solver comparison

A straightforward comparison was carried out to assess which of the two-dimensional solvers would be more appropriate for GLOF simulation. The comparison comprised the simulation of a single dam-breach hydrograph across a reconstructed DTM of the Langmoche Khola (Fig. 5). A 4 m^2 grid discretisation was used, in conjunction with a 0.1 s and 0.04 s time step for the ADI and TVD schemes, respectively (following guidance in the model documentation). A global Manning's n roughness coefficient of 0.05 was used and reflects a channel bed and margins composed predominantly of gravels, cobbles and large boulders, which is characteristic of floodplains in alpine settings. The spatial resolution of the valley-floor grid was finer than that used for subsequent probabilistic GLOF mapping, and was intended to represent the finest amount of topographic complexity on the floodplain. An ASTER GDEM-derived digital elevation model

ESURFD
2, 477–533, 2014

(corrected for vertical inaccuracy) was appended to the downstream boundary of the SfM-derived DTM of the Langmoche Khola in order to allow water to exit the domain of interest unimpeded and eliminate any artificial upstream tailwater effects.

Routing of a breach hydrograph of 5 h duration took approximately 2.5 and 0.5 h of simulation time for the TVD and ADI solvers, respectively. The computational burden of the ISIS 2-D TVD solver far exceeds that of the ADI scheme for identical model setups, owing to the finer temporal resolution required by the TVD solver. Depth-based inundation maps for the results of each solver were created in ISIS Mapper® and exported for display in ArcGIS (Fig. 6). A difference image of inundation was also created. Floodwaters follow the channel thalweg for both solvers during the 1 h. Thereafter, increasing flow stage results in the inundation of a wide reach between 1.1–1.7 km. Total inundation of this particular reach is achieved by 1:15 h for the ADI solver, and ~ 2:00 h for the TVD solver. In the early stages of the GLOF (0–45 min), the travel distance of the flood wave front is slightly greater for the TVD solver. After 1 h, areas of floodplain inundated exclusively by the TVD code are confined to a zone immediately south of the moraine breach. This difference becomes increasingly evident following the onset of floodwater recession (~ 3 h onwards).

The inundated area is greater for the ADI solver for all time steps (Fig. 6). Maximum difference in inundation extent (122 816 m^2) coincides with the upstream flood peak at 2.5 h. Significant dynamic differences also arise between the two solvers. The most prominent of these is the onset of severe oscillatory behaviour from an early stage (~ 0.5 h) in the ADI data (Fig. 6). These oscillations, which are represented by discrete, arcuate "waves" of excessive flow depth (often > 10 m) are oriented perpendicular to flow, span the entire width of the main channel in places and occur at regularly spaced intervals. These features in fact signify dramatic numerical oscillations in the ADI code (e.g. Meselhe and Holly, 1997; Venutelli et al., 2002). In contrast, the TVD data reproduce flow channelization far more clearly, apparently free of any significant oscillatory behaviour.

ESURFD
2, 477–533, 2014

Our results support the use of the two-dimensonal TVD solver for GLOF simulation. The lack of any significant numerical instability, otherwise prevalent in the ADI results, is the predominant advantage of the TVD solver. Although processing times are considerably lengthier for the TVD solver, these were deemed acceptable. We note that the solver used in this study simulates only clear-water flows, with no consideration of sediment entrainment, transfer and depositional dynamics, including any impact on flow rheology. In addition, the DTM that was used to represent the floodplain domain immediately downstream of the moraine dam reflects post-GLOF valley-floor topography. As such, derived maps of inundation and flow depth should not be taken as indicative of the passage of the 1985 GLOF.

5.2 Dam-breach modelling

5.2.1 Model evaluation

Simulations that were deemed non-behavioural (Sect. 4.3.2) were assigned a likelihood value of 0, and not considered for further analysis (Table 2). Analysis of parameter-specific likelihood data reveal that weak correlations exist for all input parameters except Manning's n (Fig. 7), although this inverse relationship is evident only for the first and second likelihood measures. Near-identical relationships were identified for all additional, perturbation-focused scenarios. Behavioural parameter ensembles possessed a low range of peak discharge (Q_p) values relative to the entire range of unconditioned data; maximum non-behavioural Q_p values exceeded $18\,000\,m^3\,s^{-1}$ for most scenarios, whereas maximum behavioural Q_p was found typically to be approximately $\sim 2000\,m^3\,s^{-1}$ (Fig. 10). Whilst the number of simulations retained for the overtopping scenarios was broadly similar, the rather more extended range possessed by the instantaneous mass-failure scenarios reflects an inverse correlation between the initial volume of material removed and number of simulations retained as behavioural. Full hydrographs were obtained for each of the retained simulations. The range of behavioural

ESURFD
2, 477–533, 2014

peak discharges of similar magnitude to previous estimates provided for the Dig Tsho GLOF (Vuichard and Zimmerman, 1987; Cenderelli and Wohl, 2001, 2003) and are of equivalent or lower magnitude to palaeo-GLOFs reported from other regions (e.g. Clague and Evans, 2000; Kershaw et al., 2005; Worni et al., 2012).

Maximum and minimum behavioural likelihood scores after the data had been conditioned using the RMSE of modelled elevation profile of the breach thalweg varied from 0.97 to 0.014. Within this range, the distribution of likelihood scores was comparable for the control scenario and all overtopping scenarios (0.970, 0.969, 0.969 and 0.970 for *DT_control* and min, mid and max overtopping scenarios respectively). Whilst the maximum likelihood for *DT_instant_1* was almost equally as high (.821), this value decreases with increasing volume of mass removed (0.819 and 0.744 for *DT_instant_3* and *DT_instant_5*). All of these scenarios possessed minimum likelihood scores that were appreciably lower than the control and overtopping scenarios. Within these ranges, likelihoods were distributed relatively evenly. Accordingly, the instantaneous mass-removal scenarios, particularly *DT_instant_3* and *DT_instant_5* exhibited the poorest performance against this likelihood function.

Behavioural elevation profiles are displayed in Fig. 8. The well-defined break in slope which is identifiable in the observed data at ∼ 550 m is reproduced by the output from HR BREACH. However, HR BREACH almost consistently underestimates the distance along the breach at which this break occurs. The majority of modelled profiles in the behavioural *DT_instant_3 and DT_instant_5* simulations are located ∼ 50–100 m further upstream than the equivalent SfM-derived, observed profile (Fig. 8). It is unclear why this systematic underestimation occurs, although an important consideration is that the observed centreline profile, viewed from above, is not linear. Instead, the breach thalweg meanders along its length, having exploited localised weaknesses in the degrading dam structure and breach flow dynamics as it developed. Consequently, the observed and modelled profiles are not truly comparable, introducing a fundamental source of error into the resulting likelihood scores (and also accounting for the discrete zone of variance between 300–370 m on all plots, Fig. 8).

ESURFD
2, 477–533, 2014

Modelled planforms are broadly similar in form both between and within each scenario (Fig. 9). Observed and modelled planforms gradually taper towards a flow constriction, beyond which the breach width expands to form a bell-shaped exit. Flow-constriction location varies considerably, with a substantial number of parameter ensembles deemed non-behavioural following conditioning using this likelihood measure (Table 2).

The majority of non-behavioural simulations located the flow constriction upstream of the behavioural limit (Fig. 9). However, no discernible relationship between input parameters and flow constriction location was identified in the parameter-specific likelihood data. Only seven *DT_control* parameter ensembles were retained (0.7 % of the original simulation pool), following conditioning on this likelihood measure, and only two (0.2 %) of the *DT_instant_5* simulations remained. Further reductions in the number of retained simulations were imposed for all scenarios (Table 2).

5.2.2 Percentile hydrograph extraction

CDF curves were extracted from behavioural, scenario-specific likelihood data (Fig. 4). Using these data, time step-specific percentile discharges were extracted and combined to construct probabilistic breach outflow hydrographs for each scenario (Fig. 10). Similarities between the percentile hydrographs for each scenario are striking, particularly between data conditioned on modelled final breach depth (LH1) and modelled final breach depth and breach centreline elevation profile data (LH1 + 2). All 95th percentile hydrographs possess steep rising limbs, comparatively shallower falling limbs, and generally trace the upper boundary of the behavioural hydrograph envelope. Exceptions to this rule are *DT_overtop_min*, *DT_overtop_max* and *DT_instant_1*, whose hydrographs dip below this upper bound by a noticeable margin. *DT_instant_3* and *DT_instant_5* possess shorter duration hydrographs; a direct consequence of the form of the behavioural envelope from which the CDF were derived. Shortening of the hydrograph duration results in greater concentration of all percentile hydrographs for these

ESURFD
2, 477–533, 2014

scenarios, with the result being reduced variation in percentile-specific Q_p and Q_{vol} (Table 3).

Individual overtopping waves are preserved for each percentile in the relevant scenarios (Fig. 10). Median (50th) percentile hydrographs exhibit slightly more variation, both between scenarios, and following conditioning using the second likelihood measure. This conditioning step results in a decrease in median percentile Q_p for control and overtopping scenarios, but has a negligible effect on the mass-removal simulations (Fig. 10). For all scenarios, 5th percentile hydrographs generally trace the lower boundary of the behavioural hydrograph envelope, and appear to be largely unaffected by additional conditioning using the elevation profile of the breach centreline.

The most noticeable impact on percentile hydrograph form is caused by the additional conditioning of the data on the final likelihood measure. Mass-removal scenarios appear to be affected to a far lesser degree than the control and overtopping scenarios. The exception is *DT_instant_5*, where discharges for 50th and 5th percentile hydrographs are increased in the first ~ 80 min, and after which 95th percentile discharges decrease, resulting in substantial concentration of the percentile hydrographs (Fig. 10). Conditioning on this final likelihood measure causes increased Q_p for *DT_overtop_min* and *DT_overtop_mid* median percentile hydrographs, whilst the hydrograph for *DT_overtop_max* is perturbed between 140–200 min. Notably, *DT_control* exhibits increased discharges for the 5th and 50th percentiles, coupled with decreased Q_p and steepening of the falling limb of the 95th percentile hydrograph.

Crucially, percentile hydrograph form is dictated by the time step-specific CDF data. In turn, CDF form is determined by variations in the likelihood of individual behavioural hydrographs, and the cumulative distribution of their associated discharges (for each time step). The vast number of simulations which, following conditioning on flow constriction location, were subsequently deemed to be non-behavioural (Table 1) serves to alter the form of scenario-specific CDFs. This effect is particularly dramatic for *DT_control*, where the number of behavioural simulations reduces from 76 to 7 following conditioning on final breach depth, breach centreline elevation profile, and flow

ESURFD
2, 477–533, 2014

constriction location (LH1 + 2 + 3). Similarly, CDF data for *DT_instant_5* are derived from just two behavioural hydrographs, which explains both the smaller hydrograph envelope and the high concentration of the percentile hydrographs (Fig. 10).

5.2.3 Data clustering

Issues of mass conservation arose with the extraction of behavioural, percentile-derived breach hydrographs. Both 5th and 50th percentile hydrographs for all scenarios consistently under-predicted the volume of lake water released during breach development ($\sim 7.3 \times 10^6$ m^3), whereas volumetric integration of 95th percentile hydrograph data produced substantially increased values of Q_{vol} (Table 3). The median percentile performs best at replicating total flood volume, under-predicting Q_{vol} by between 0.2–0.7×10^6 m^3, 0.4–0.7×10^6 m^3 and 0.1–1.3×10^6 m^3 for LH1, LH1 + 2, and LH1 + 2 + 3, respectively (Table 3).

From a hydrodynamic modelling perspective, an additional and equally important observation is the form of the percentile hydrographs, which generally do not mirror the form of any of the behavioural hydrographs used as input. Combined, issues of mass conservation, and the unrepresentative form of the percentile breach hydrographs render them largely unsuitable for use as an upstream boundary condition for subsequent hydrodynamic modelling.

In an effort to further refine the behavioural simulations and improve the representativeness of the derived percentile hydrographs, all behavioural data were clustered, regardless of their inclusion of any modelled system perturbations (Fig. 11). Data clustering was undertaken in an effort to characterise "styles" of breaching (for example, low peak discharge magnitude and lengthy time to peak, or high peak discharge and short, sharp, rise to peak) using Q_p and T_p data, and independent of the various breaching scenarios that were modelled. An automated, subtractive clustering algorithm was applied to the unified Q_p and time to peak (T_p) data. This method identifies natural cluster centroids in raw point datasets, and quantifies the density of points relative to one another. Each point is assumed to represent a potential cluster centroid and a measure

ESURFD
2, 477–533, 2014

of likelihood is calculated, based on the density of surrounding points. Following initial cluster identification, the density function is revised and subsequent cluster centres identified in the same manner until a sufficient number of natural clusters are deemed to have been obtained (Hammouda and Karray, 2000; Mathworks, 2012). Point-cluster membership was determined by calculation of the minimum Euclidean distance between each data-point and cluster centre. The subtractive method eliminates any subjectivity associated with manual cluster identification.

Clusters are broadly defined by T_p range. Cluster 1 contains all simulations with T_p of approximately 60–130 min, Cluster 2 is defined by T_p of ~ 130–170 min, and Cluster 3 possesses T_p values in the range ~ 170–270 min. Ranges of Q_p overlap substantially between Cluster 1 and Cluster 2 (~ 900–2100 $m^3 s^{-1}$, and ~ 700–1800 $m^3 s^{-1}$, respectively), and to a lesser degree between Cluster 2 and Cluster 3. These clusters may be taken as approximately representing a number of "types" of breach hydrograph, namely: (relatively) high-magnitude, short-duration (Cluster 1), moderate peak magnitude and mid-range duration (Cluster 2) and low-magnitude, extended duration (Cluster 3) GLOF hydrographs.

Cluster membership, is not as clear-cut as might be anticipated (Fig. 11). The clustering results appear to imply that pigeonholing different breaching scenarios by hydrograph type, or style, is virtually impossible. However, the exceptions to this rule are the instantaneous mass-removal scenarios, which almost exclusively produce high-magnitude, short-duration hydrographs. This finding would appear to imply that alternative factors are required to explain the similarity in the range of hydrograph forms that are produced by each scenario.

Percentile hydrographs were also extracted from the clustered data. Deviations between observed and modelled median percentile Q_{vol} data are in the range −41 to −6 %, demonstrating a minimal improvement over unclustered and scenario-specific values of modelled Q_{vol} (Table 3). Clustered 5th and 95th percentile Q_{vol} data vastly under- and over-estimate observed Q_{vol}.

ESURFD
2, 477–533, 2014

Clustering was largely unsuccessful at improving the utility of percentile-based breach hydrographs for use as hydrodynamic input, thereby necessitating the exploration of alternative methods for cascading likelihood-weighted estimates of dam-breach parameter ensemble performance through to the simulation and mapping of GLOF inundation and hazard.

5.3 Hydrodynamic modelling

5.3.1 The optimal hydrograph

Deterministic approaches to flood reconstruction require the identification of the optimal model, and its subsequent use for predictive flood forecasting. To illustrate the variability between scenario-specific optimal hydrograph routing patterns, the optimal hydrographs for *DT_control*, *DT_overtop_max* and *DT_instant_5* were used as upstream input for simulation in ISIS 2-D. Maps of inundation extent and flow depth (Fig. 12) reveal prominent inter-scenario differences in the spatial extent of inundation as the respective hydrographs and GLOF floodwaters progress downstream. Variations of note include the initial downstream transmission of the *DT_overtop_max* overtopping wave, which triggers rapid inundation of the entire reach (Fig. 12). However, initially high flow stages are not maintained, and only rise once again with increasing breach discharge associated with breach expansion. Use of the *DT_instant_5* hydrograph produces spatial and temporal patterns of inundation and wetting front travel time similar to that of *DT_overtop_max* (Fig. 12).

5.3.2 GLUE-based GLOF reconstruction

Probabilistic maps of inundation extent and flow depth were constructed through the retention and evaluation of scenario-specific and likelihood-weighted breach hydrographs. In the example presented herein, we simulated the propagation of 76 individual moraine-breach hydrographs using the ISIS 2-D TVD solver (with an 8 m topographic

ESURFD
2, 477–533, 2014

grid discretisation and a 0.04 s time step), representing the behavioural *DT_control* parameter ensembles after conditioning on final breach depth. However, the method is equally applicable to the use of several, hundreds, or thousands of individual simulations. For each time step, Per-cell CDF curves of flow depth were assembled, from which percentile flow depths were extracted and plotted (Fig. 13). Given the inherent uncertainty surrounding the precise mode of moraine-dam failure and outflow hydrograph form, these data effectively convey the resulting variability in likelihood-weighted predictions of reconstructed inundation extent, whilst preserving time step-specific percentile flow depths. Due to the nature of their construction, these data do not relate to a specific event or hydrograph, but instead provide an indication as to the potential uncertainty in GLOF inundation extents and flow depths associated with a range of behavioural breach hydrographs.

5.3.3 Probabilistic hazard mapping

The final output of a GLOF hazard assessment comprises the production of maps of flood hazard, conditioned by one or more directly-quantifiable flood-intensity indicators (e.g. Aronica et al., 2012). Whilst inundation depth is arguably the most significant flood-intensity indicator for predicting monetary losses associated with individual flood events (Merz and Thieken, 2004; Vorogushyn et al., 2010, 2011), its combination with flow velocity is regarded as an improved indicator of hazard to human life (Aronica et al., 2012).

A global hazard index proposed by Aronica et al. (2012) was used to construct maps of GLOF hazard (Fig. 14). Taking probabilistic flow depth and velocity data as input, probabilistic GLOF hazard maps were produced for the *DT_control* scenario. Four hazard classes are defined and shaded for distinction (H_1 to H_4; in order of increasing hazard). Hazard distribution is characterised by extensive zones of H_1 for the 5th and 50th percentiles in the first 0.5 h, with higher hazard classes becoming increasingly prevalent in the 95th percentile data (Fig. 14). As breach outflow increases and the maximum inundation extent is approached, the zone immediately adjacent to the channel

ESURFD
2, 477–533, 2014

thalweg is classed as "very high" (H_4) hazard, and is associated with flow depths in excess of 1.5 m and regardless of velocity. Classes H_1, H_3 and H_4 dominate for all time steps, whilst H_2 is noticeably underrepresented. Inundated channel-marginal areas are generally classed as being of low hazard, whilst the classification of the remaining inundated area as H_3 or H_4 indicates the presence of flow velocities that either exceed the prescribed product of depth and velocity ($0.7\,m^2\,s^{-1}$), or depths in excess of 1.5 m.

6 Discussion

6.1 Elucidating the key controls on breach development

The inherent uncertainty associated with moraine dam-breach model parameterisation has a significant influence on the magnitude and characteristics of modelled breach hydrographs. This has significant implications for GLOF reconstruction efforts, and particularly for subsequent hydrodynamic modelling. We have demonstrated that the propagation, or cascading, of the parametric uncertainty and equifinality through the dam-breach and hydrodynamic modelling elements of the GLOF model chain is not only possible, but may be of considerable value to flood risk practitioners. The methodological framework developed and demonstrated in this study is summarised in Fig. 15.

Our results highlight the primary influence of moraine material roughness in dictating HR BREACH parameter ensemble (and therefore breach hydrograph) performance. Specifically, behavioural Manning's n coefficients were found to be in the range 0.020–$0.029\,m^{-1/3}\,s$ (Fig. 7), representing a significant refinement of the a priori parameter range (0.02–$0.05\,m^{-1/3}\,s$). In contrast, no significant refinement of the remaining material characteristic parameters was made following model evaluation.

However, posterior Manning's n values appear to be highly unrealistic; the Dig Tsho moraine is composed predominantly of gravel-, cobble- and boulder-sized material, which is more likely to be associated with larger roughness coefficient values (Chow, 1959). Precisely why this occurs is unclear. However, the physicality of the numerical

ESURFD
2, 477–533, 2014

dam-breach model used in this research undoubtedly represents an improvement over empirical or analytical models. It should also be noted that many of the geometric and material characteristics of the moraine and lake complex remain highly simplified.

6.2 The utility of behavioural GLOF modelling

The computational restrictions that dominate both the recovery of high-resolution topographic moraine and valley-floor data and the use of higher-order hydrodynamic codes were appreciable in this study, where access to a suite of powerful computing resources was not an issue. However, options for streamlining the framework are being considered. The most computationally-demanding step in the model chain is currently the two-dimensional hydrodynamic modelling component. Consequently, one avenue for exploration might be the use of reduced-complexity hydrodynamic codes, which preserve much of the physicality of "full" 2-D codes, but at a much-reduced computational burden (e.g. McMillan and Brasington, 2007; Yu and Lane, 2006).

Whilst the extraction of percentile maps of inundation extent and flow depth is not necessarily an entirely new concept (e.g. McMillan and Brasington, 2007, 2008; Vorogusyhn et al., 2010, 2011), the application to GLOF reconstruction presented here is an original and novel one. This approach represents a significant improvement in the effective communication of the likelihood associated with a range of moraine-dam failure scenarios, and the production of meaningful, probability-based flood hazard maps.

The likelihood of multiple GLOFs occurring from an individual moraine-dammed lake complex is extremely low, since in the majority of cases, the breached moraine dam can comfortably accommodate relict lake discharges. Therefore, the identification and use of posterior parameter distribution data for predictive GLOF forecasting is of limited utility if these ranges prove to be highly site-specific (which this additional data would appear to suggest). Ultimately, the identification of a suite of universal or region-specific material characteristics and their probabilistic distributions would facilitate their use in predictive GLOF simulation efforts, and should be a focus of future research.

ESURFD
2, 477–533, 2014

In considering the source of uncertainty in the GLOF modelling process, we have focused on its influence over the moraine dam-failure process. However, numerous additional sources of uncertainty are present at various stages in the workflow (e.g. reconstruction of drained lake-basin bathymetry and extraction of hypsometric data) and merit further investigation (Westoby et al., 2014). The logistical impracticalities of identifying and addressing all sources of uncertainty in the GLOF model chain are likely to prove a significant hindrance to applied modelling efforts. However, simple sensitivity analyses remain of value to quantify the impacts of individual sources of uncertainty on numerical dam-breach and hydrodynamic simulation, and might be incorporated straightforwardly into the framework (Fig. 15).

Probabilistic approaches have clear advantages over the deterministic approaches traditionally used for GLOF reconstruction such as the use of paleohydraulic techniques for at-a-point, or reach-scale peak discharge estimation (e.g. Cenderelli and Wohl, 2003; Kershaw et al., 2005; Bohorquez and Darby, 2008). Probabilistic methods embrace and attempt to convey the influence of uncertainty and equifinality in model input on subsequent output, and it might be argued that their value outweighs the additional processing time required for their implementation, which may involve the execution of hundreds or thousands of individual simulations.

7 Conclusions

This paper has outlined and presented results from a workflow for cascading uncertainty and equifinality through the Glacial Lake Outburst Flood (GLOF) model chain using a combination of advanced, physically-based numerical dam-breach and hydrodynamic models. Dam material roughness is the dominant influence on outflow hydrograph form. We have demonstrated that morphological characteristics of a GLOF breach are appropriate measures for assessing the performance of individual simulations, or parameter ensembles, at reproducing observed breach morphology. Breach morphology is reproducible by parameter ensembles associated with differing breach

ESURFD
2, 477–533, 2014

initiation scenarios, lending support for the adoption of probabilistic, as opposed to deterministic methods for dam-breach outburst flood reconstruction. We also demonstrate an effective approach for cascading dam-breach simulation likelihood data through to the construction of probability-based maps of GLOF inundation extent and flow depth, and the subsequent derivation of event-specific maps of flood hazard. Future research should focus on the suitability of probabilistic methods for predictive, as opposed to reconstructive, GLOF simulation and hazard assessment.

Acknowledgements. MJW was funded by a NERC Open CASE Award (NE/G011443/1) in partnership with Reynolds International Ltd. Additional funding to support field activities from the Department of Geography and Earth Sciences Postgraduate Discretionary Fund (Aberystwyth University) is duly acknowledged. J. Balfour, P. Cowley, S. Doyle, H. Sevestre, C. Souness, R. Taylor and guides and porters from Summit Trekking, Kathmandu, assisted with data collection in the Khumbu Himal. HR Wallingford Ltd and the Halcrow Group Ltd are thanked for the provision of academic licences for the use of HR BREACH and ISIS 2D, respectively. GeoEye imagery (Fig. 1b) was provided free of charge by the GeoEye Foundation. ASTER GDEM data were downloaded free of charge from http://asterweb.jpl.nasa.gov/gdem.asp. Breach hydrograph data clustering was undertaken in MathWorks' MATLAB®.

References

Alho, P. and Aaltonen, J.: Comparing a 1D hydraulic model with a 2D hydraulic model for the simulation of extreme glacial outburst floods, Hydrol. Process., 22, 1537–1547, 2008.

Aronica, G., Hankin, B., and Beven, K.: Uncertainty and equifinality in calibrating distributed roughness coefficients in a flood propagation model with limited data, Adv. Water Resour., 22, 349–365, 1998.

Aronica, G., Bates, P. D., and Horritt, M. S.: Assessing the uncertainty in distributed model predictions using observed binary pattern information within GLUE, Hydrol. Process., 16, 2001–2016, 2002.

Aronica, G., Candela, A., Fabio, P., and Santoro, M.: Estimation of flood inundation probabilities using global hazard indexes based on hydrodynamic variables, Phys. Chem. Earth, 42–44, 119–129, 2012.

ESURFD

2, 477–533, 2014

Astre, H.: SFMToolkit3, available at: http://www.visual-experiments.com/demos/sfmtoolkit (last access: 12 June 2014), 2010.
Bajracharya, B., Shrestha, A. B., and Rajbhandar, L.: Glacial Lake Outburst Floods in the Sagarmatha Region, Mt. Res. Dev., 27, 336–344, 2007.
Barré de St-Venant, A. J. C.: Théorie et Equations Générales du Mouvement Non Permanent des Eaux Courantes, Comptes Rendus des séances de l'Académie des Sciences, 73, 147–154, 1871.
Bates, P. D., Marks, K. J., and Horritt, M. S.: Optimal use of high-resolution topographic data in flood inundation models, Hydrol. Process., 17, 537–557, 2003.
Benn, D. I., Wiseman, S., and Hands, K. A.: Growth and drainage of supraglacial lakes on debris-mantled Ngozumpa Glacier, Khumbu Himal, Nepal, J. Glaciol., 47, 626–638, 2001.
Benn, D. I., Bolch, T., Hands, K., Gulley, J., Luckman, A., Nicholson, L. I., Quincey, D. J., Thompson, S., Toumi, R., and Wiseman, S.: Response of debris-covered glaciers in the Mount Everest region to recent warming and implications for outburst flood hazards, Earth-Sci. Rev., 114, 156–174, 2012.
Beven, K.: A manifesto for the equifinality thesis, J. Hydrol., 320, 18–36, 2005.
Beven, K. and Binley, A.: The future of distribution models: model calibration and uncertainty prediction, Hydrol. Process., 6, 279–298, 1992.
Beven, K. and Freer, J.: Equifinality, data assimilation, and uncertainty estimation in mechanistic modelling of complex environmental systems using the GLUE methodology, J. Hydrol., 249, 11–29, 2001.
Blazkova, S. and Beven, K.: Flood frequency estimation by continuous simulation of subcatchment rainfalls and discharges with the aim of improving dam safety assessment in a large basin in the Czech Republic, J. Hydrol., 292, 153–172, 2004.
Bohorquez, P. and Darby, S. E.: The use of one- and two-dimensional hydraulic modelling to reconstruct a glacial outburst flood in a steep Alpine valley, J. Hydrol., 361, 240–261, 2008.
Bolch, T., Pieczonka, T., and Benn, D. I.: Multi-decadal mass loss of glaciers in the Everest area (Nepal Himalaya) derived from stereo imagery, The Cryosphere, 5, 349–358, doi:10.5194/tc-5-349-2011, 2011.
Bolch, T., Kulkarni, A., Kääb, A., Huggel, C., Paul, F., Cogley, J. G., Frey, H., Kargel, J. S., Fujita, K., Scheel, M., Bajracharya, S., and Stoffel, M.: The state and fate of Himalayan glaciers, Science, 336, 310–314, 2012.

ESURFD
2, 477–533, 2014

Cameron, D.: Flow, frequency, and uncertainty estimation for an extreme historical flood event in the Highlands of Scotland, UK, Hydrol. Process., 21, 1460–1470, 2007.
Cao, Z. and Carling, P.: Mathematical modelling of alluvial rivers: reality and myth, Part 1: general overview, Mar. Eng., 154, 207–219, 2002.
Casas, A., Lane, S. N., Yu, D., and Benito, G.: A method for parameterising roughness and topographic sub-grid scale effects in hydraulic modelling from LiDAR data, Hydrol. Earth Syst. Sci., 14, 1567–1579, doi:10.5194/hess-14-1567-2010, 2010.
Castellarin, A., Merz, R., and Bloschl, G.: Probabilistic envelope curves for extreme rainfall events, J. Hydrol., 378, 263–271, 2009.
Cenderelli, D. A. and Wohl, E. E.: Peak discharge estimates of glacial-lake outburst floods and "normal" climatic floods in the Mount Everest region, Nepal, Geomorphology, 40, 57–90, 2001.
Cenderelli, D. A. and Wohl, E. E.: Flow hydraulics and geomorphic effects of glacial-lake outburst floods in the Mount Everest region, Nepal, Earth Surf. Proc. Land., 28, 385–407, 2003.
Chen, Y. H. and Anderson, B. A.: Development of a methodology for estimating embankment damage due to flood overtopping, US Federal Highway Administration Report No, FHWA/RD-86/126, 1986.
Chow, V. T.: Open-Channel Hydraulics, McGraw-Hill, New York, 677 pp., 1959.
Clague, J. J. and Evans, S. G.: A review of catastrophic drainage of moraine-dammed lakes in British Columbia, Quaternary Sci. Rev., 19, 1763–1783, 2000.
Dewals, B., Erpicum, S., Detrembleur, S., Archambeau, P., and Pirotton, M.: Failure of dams arranged in series or in complex, Nat. Hazards, 56, 917–939, 2011.
Di Baldassarre, G. and Claps, P.: A hydraulic study on the applicability of flood rating curves, Hydrol. Res., 42, 10–19, 2011.
Fonstad, M. A., Dietrich, J. T., Courville, B. C., Jensen, J. L., and Carbonneau, P. E.: Topographic structure from motion: a new development in photogrammetric development, Earth Surf. Proc. Land., 38, 421–430, 2013.
Franz, K. J. and Hogue, T. S.: Evaluating uncertainty estimates in hydrologic models: borrowing measures from the forecast verification community, Hydrol. Earth Syst. Sci., 15, 3367–3382, doi:10.5194/hess-15-3367-2011, 2011.
Freer, J., Beven, K. J., and Peters, N. E.: Multivariate seasonal period model rejection within the generalised likelihood uncertainty estimation procedure, in: Calibration of Watershed Models,

ESURFD
2, 477–533, 2014

edited by: Duan, Q., Gupta, H., Sorooshian, S., Rousseau, A. N., and Turcotte, R., AGU Books, Washington, 69–87, 2002.
Frey, H., Haeberli, W., Linsbauer, A., Huggel, C., and Paul, F.: A multi-level strategy for anticipating future glacier lake formation and associated hazard potentials, Nat. Hazards Earth Syst. Sci., 10, 339–352, doi:10.5194/nhess-10-339-2010, 2010.
Galay, V.: Glacier Lake Outburst Flood (Jökulhlaup) on the Bothe/Dudh Kosi, 4 August 1985. Internal Report, Water and Energy Committee, Ministry of Water Resources, His Majesty's Government of Nepal, Kathmandu, Nepal, 1985.
Halcrow: ISIS 2D by Halcrow, overview available at: www.halcrow.com/isis/ (last access: 12 June 2014), 2012.
Hall, J., Tarantola, S., Bates, P. D., and Horritt, M.: Distributed sensitivity analysis of flood inundation model calibration, J. Hydraul. Eng., 131, 117–126, 2005.
Hanson, G. J. and Cook, K. R.: Apparatus, test procedures, and analytical methods to measure soil erodibility in situ, Appl. Eng. Agric., 20, 455–462, 2004.
Harrison, S., Glasser, N. F., Winchester, V., Haresign, E., Warren, C., and Jansson, K.: A glacial lake outburst flood associated with recent mountain glacier retreat, Patagonian Andes, Holocene, 16, 611–620, 2006.
Hassan, A. E., Bekhit, H., and Chapman, J. B.: Uncertainty assessment of a stochastic groundwater flow model using GLUE analysis, J. Hydrol., 362, 89–109, 2008.
Hassan, M. and Morris, M.: HR-BREACH Model Documentation, HR Wallingford Ltd, Wallingford, Oxfordshire, UK, 2012.
Horritt, M. S. and Bates, P. D.: Evaluation of 1D and 2D numerical models for predicting river flood inundation, J. Hydrol., 268, 87–99, 2002.
Hunter, N. M., Bates, P. D., Horritt, M. S., De Roo, A. P. J., and Werner, M. G. F.: Utility of different data types for calibrating flood inundation models within a GLUE framework, Hydrol. Earth Syst. Sci., 9, 412–430, doi:10.5194/hess-9-412-2005, 2005.
Iman, R. L. and Helon, J. C.: An investigation of uncertainty and sensitivity analysis techniques for computer models, Risk Anal., 8, 71–90, 2006.
IMPACT: Investigation of Extreme Flood Processes and Uncertainty: Risk and Uncertainty (WP5) – Technical Report, 44 pp., available at: www.impact-project.net (last access: 12 June 2014), 2004.

ESURFD
2, 477–533, 2014

James, M. R. and Robson, S.: Straightforward reconstruction of 3D surfaces and topography with a camera: accuracy and geoscience applications, J. Geophys. Res., 117, F03017, doi:10.1029/2011JF002289, 2012.
Janský, B., Engel, Z., Šobr, M., Beneš, V., Špaček, K., and Yerokhin, S.: The evolution of Petrov lake and moraine dam rupture risk (Tien-Shan, Kyrgyzstan), Nat. Hazards, 50, 83–96, 2009.
Javernick, L., Brasington, J., and Caruso, B.: Modelling the topography of shallow braided rivers using Structure-from-Motion photogrammetry, Geomorphology, 213, 166–182, doi:10.1016/j.geomorph.2014.01.006, 2014.
Kääb, A., Huggel, C., Fischer, L., Guex, S., Paul, F., Roer, I., Salzmann, N., Schlaefli, S., Schmutz, K., Schneider, D., Strozzi, T., and Weidmann, Y.: Remote sensing of glacier- and permafrost-related hazards in high mountains: an overview, Nat. Hazards Earth Syst. Sci., 5, 527–554, doi:10.5194/nhess-5-527-2005, 2005.
Kaser, G., Cogley, J. G., Dyurgerov, B., Meier, M. F., and Ohmura, A.: Mass balance of glaciers and ice caps: consensus estimates for 1961–2004, Geophys. Res. Lett., 33, 1–5, 2006.
Kershaw, J. A., Clague, J. J., and Evans, S. G.: Geomorphic and sedimentological signature of a two-phase outburst flood from moraine-dammed Queen Bess Lake, British Columbia, Canada, Earth Surf. Proc. Land., 30, 1–25, 2005.
Kidson, R. L., Richards, K. S., and Carling, P. A.: Hydraulic model calibration for extreme floods in bedrock-confined channels: case study from northern Thailand, Hydrol. Process., 20, 329–344, 2006.
Kuczera, G. and Parent, E.: Monte Carlo assessment of parameter uncertainty in conceptual catchment models: the Metropolis algorithm, J. Hydrol., 211, 69–85, 1998.
Lamb, R., Beven, K., and Myrabo, S.: Use of spatially distributed water table observations to constrain uncertainty in a rainfall–runoff model, Adv. Water Resour., 22, 305–317, 1998.
Lebourg, T., Riss, J., and Pirard, E.: Influence of morphological characteristics of heterogeneous moraine formations on their mechanical behaviour using image and statistical analysis, Eng. Geol., 73, 37–50, 2004.
Liang, D., Falconer, R. A., and Lin, B.: Comparison between TVD-MacCormack and ADI-type solvers of the shallow water equations, Adv. Water Resour., 29, 1833–1845, 2006.
Liang, D., Lin, B., and Falconer, R. A.: Simulation of rapidly varying flow using an efficient TVD-MacCormack scheme, Int. J. Numer. Method. H., 53, 811–826, 2007.
Liao, C. B., Wu, M. S., and Liang, S. J.: Numerical simulation of a dam break for an actual river terrain environment, Hydrol. Process., 21, 447–460, 2007.

ESURFD
2, 477–533, 2014

Lliboutry, L., Morales, B., Pautre, A., and Schneider, B.: Glaciological problems set by the control of dangerous lakes in Cordillera Blanca, Peru, I: Historical failure of morainic dams, their causes and prevention, J. Glaciol., 18, 239–254, 1977.
Lowe, D. G.: Distinctive image features from scale-invariant keypoints, Int. J. Comput. Vision, 60, 91–110, 2004.
Mathworks®: MATLAB (version 7.6), available at: www.mathworks.co.uk 2012.
McMillan, H. K. and Brasington, J.: Reduced complexity strategies for modelling urban floodplain inundation, Geomorphology, 90, 226–243, 2007.
McMillan, H. K. and Brasington, J.: End-to-end flood risk assessment: a coupled model cascade with uncertainty estimation, Water Resour. Res., 44, W03419, doi:10.1029/2007WR005995, 2008.
Merz, B. and Thieken, A.: Flood risk analysis: concepts and challenge, Oesterreeichische Wasser Abfallwirtscht, 56, 27–34, 2004.
Meselhe, E. A. and Holly Jr., F. M.: Invalidity of Preissmann scheme for transcritical flow, J. Hydraul. Eng., 123, 652–655, 1997.
Metropolis, N.: The beginning of the Monte Carlo method, Los Alamos Science, 1987 Special Issue, 125–130, 1987.
Mohamed, M. A. A., Samuels, P. G., Morris, M., and Ghataora, G. S.: Improving the accuracy of prediction of breach formation through embankment dams and flood embankments, in: River Flow 2002: 1st International Conference on Fluvial Hydraulics, edited by: Bousmar, D. and Zech, Y., Louvain-la-Neuve, Belgium, 3–6 September, 10 pp., 2002.
Morris, M., Hanson, G., and Hassan, M. A. A.: Improving the accuracy of breach modelling: why are we not progressing faster?, J. Flood Risk Manage., 1, 150–161, 2008.
Nicholas, A. P. and Quine, T. A.: Quantitative assessment of landform equifinality and palaeoenvironmental reconstruction using geomorphic models, Geomorphology, 121, 167–183, 2010.
Oerlemans, J.: Quantifying global warming from the retreat of glacier, Science, 264, 243–245, 1994.
Osti, R. and Egashira, S.: Hydrodynamic characteristics of the Tam Pokhari Glacial Lake outburst flood in the Mt. Everest region, Nepal, Hydrol. Process., 23, 2943–2955, 2009.
Osti, R., Bhattarai, T. N., and Miyake, K.: Causes of catastrophic failure of Tam Pokhari moraine dam in the Mt. Everest region, Nat. Hazards, 58, 1209–1223, 2011.
Pappenberger, F., Beven, K. J., Hunter, N. M., Bates, P. D., Gouweleeuw, B. T., Thielen, J., and de Roo, A. P. J.: Cascading model uncertainty from medium range weather forecasts

ESURFD
2, 477–533, 2014

(10 days) through a rainfall-runoff model to flood inundation predictions within the European Flood Forecasting System (EFFS), Hydrol. Earth Syst. Sci., 9, 381–393, doi:10.5194/hess-9-381-2005, 2005.
Pappenberger, F., Matgen, P., Beven, K. J., Henry, J. B., Pfister, L., and Fraipont de, P.: Influence of uncertain boundary conditions and model structure on flood inundation predictions, Adv. Water Resour., 29, 1430–1449, 2006.
Parkin, G., O'Donnell, G., Ewen, J., Bathurst, J. C., O'Connell, P. E., and Lavabre, J.:Validation of catchment models for predicting land-use and climate change impacts: 2. Case study for a Mediterranean catchment, J. Hydrol., 175, 595–613, 1996.
Quincey, D. J., Lucas, R. M., Richardson, S. D., Glasser, N. F., Hambrey, M. J., and Reynolds, J. M.: Optical remote sensing techniques in high-mountain environments: application to glacial hazards, Prog. Phys. Geogr., 29, 475–505, 2005.
Quincey, D. J., Richardson, S. D., Luckman, A., Lucas, R. M., Reynolds, J. M., Hambrey, M. J., and Glasser, N. F.: Early recognition of glacial lake hazards in the Himalaya using remote sensing datasets, Global Planet. Change, 56, 137–152, 2007.
Refsgaard, J. C.: Parameterisation, calibration and validation of distributed hydrological models, J. Hydrol., 198, 69–97, 1997.
Richardson, S. D. and Reynolds, J. M.: An overview of glacial hazards in the Himalayas, Quatern. Int., 65/66, 31–47, 2000.
Rojas, R., Feyen, L., and Dassargues, A.: Conceptual model uncertainty in groundwater modelling: combing generalized likelihood uncertainty estimation and Bayesian model averaging, Water Resour. Res., 44, W12418, doi:10.1029/2008WR006908, 2008.
Romanowicz, R. and Beven, K.: Dynamic real-time prediction of flood inundation probabilities, Hydrolog. Sci. J., 43, 181–196, 1998.
Rychkov, I., Brasington, J., and Vericat, D.: Computational and methodological aspects of terrestrial surface analysis based on point clouds, Comput. Geosci., 42, 64–70, 2012.
Sakai, A., Chikita, K., and Yamada, T.: Expansion of a moraine-dammed glacial lake, Tsho Rolpa, in Rolwaling Himal, Nepal Himalaya, Limnol. Oceanogr., 45, 1401–1408, 2000.
Sanders, B. F.: Evaluation of on-line DEMs for flood inundation modelling, Adv. Water Resour., 30, 1831–1843, 2007.
Snavely, N.: Scene Reconstruction and Visualization from Internet Photo Collections, unpublished Ph.D. thesis, University of Washington, USA, 2008.

ESURFD
2, 477–533, 2014

Snavely, N., Seitz, S. N., and Szeliski, R.: Modelling the world from internet photo collections, Int. J. Comput. Vision 80, 189–210, 2008.
Spetsakis, M. E., Aloimonos, Y.: A multi-frame approach to visual motion perception, Int. J. Comput. Vision, 6, 245–255, 1991.
Stokes, C. R., Spagnolo, M., and Clark, C. D.: The composition and internal structure of drumlins: complexity, commonality, and implications for a unifying theory of their formation, Earth-Sci. Rev., 107, 398–422, 2011.
Thompson, S. S., Benn, D. I., Dennis, K., and Luckman, A.: A rapidly-growing moraine-dammed glacial lake on Ngozumpa Glacier, Nepal, Geomorphology, 145–146, 1–11, 2012.
Vasquez, R. F., Beven, K., and Feyen, J.: GLUE based assessment on the overall predictions of a MIKE SHE application, Water Resour. Manag., 23, 1325–1349, 2009.
Venutelli, M.: Stability and accuracy of weighted four-point implicit finite difference schemes for open channel flow, J. Hydraul. Eng., 128, 281–288, 2002.
von Bertalanffy, L.: General System Theory – Foundations, Development, Applications, 2nd Edn., George Braziller, New York, 295 pp., 1968.
Vorogushyn, S., Merz, B., Lindenschmidt, K. E., and Apel, H.: A new methodology for flood hazard assessment considering dike breaches, Water Resour. Res., 46, W08541, doi:10.1029/2009WR008475, 2010.
Vorogushyn, S., Apel, H., and Merz, B.: The impact of the uncertainty of dike breach development time on flood hazard, Phys. Chem. Earth, 36, 319–323, 2011.
Vrugt, J. A., ter Braak, C. J. F., Gupta, H. V., and Robinson, B. A.: Equifinality of formal (DREAM) and informal (GLUE) Bayesian approaches in hydrologic modelling?, Stoch. Env. Res. Risk A., 23, 1011–1026, 2009.
Vuichard, D., and Zimmerman, M.: The Langmoche flash-flood, Khumbu Himal, Nepal, Mt. Res. Dev., 6, 90–94, 1986.
Vuichard, D., and Zimmerman, M.: The 1985 catastrophic drainage of a moraine-dammed lake, Khumbu Himal, Nepal: cause and consequences, Mt. Res. Dev., 7, 91–110, 1987.
Wahl, T.: Prediction of embankment dam breach parameters: a literature review and needs assessment, Report no. DSO-98–004, Water Resources Research Laboratory, Dam Safety Office, Department of the Interior, 67 pp., Denver, Colorado, 1998.
Wang, W., Yang, X., and Yao, T.: Evaluation of ASTER GDEM and SRTM and their suitability in hydraulic modelling of a glacial lake outburst flood in southeast Tibet, Hydrol. Process., 26, 213–225, 2012.

ESURFD
2, 477–533, 2014

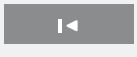

Watanabe, T. and Rothacher, D.: The 1994 Lugge Tsho Glacial Lake Outburst Flood, Bhutan Himalaya, Mt. Res. Dev., 16, 77–81., 1996.
Watanabe, T., Kameyama, S., and Sato, T.: Imja Glacier dead-ice melt rates and changes in a supraglacial lake, 1989–1994, Khumbu Himal, Nepal: danger of lake drainage, Mt. Res. Dev., 15, 293–300, 1995.
Westerberg, I. K., Guerrero, J.-L., Younger, P. M., Beven, K. J., Seibert, J., Halldin, S., Freer, J. E., and Xu, C.-Y.: Calibration of hydrological models using flow-duration curves, Hydrol. Earth Syst. Sci., 15, 2205–2227, doi:10.5194/hess-15-2205-2011, 2011.
Westoby, M. J.: The Development of a Unified Framework for Low-Cost Glacial Lake Outburst Flood Hazard Assessment, unpublished Ph.D. thesis, Department of Geography, History and Politics, Aberystwyth University, 456 pp., 2013.
Westoby, M. J., Brasington, J., Glasser, N. F., Hambrey, M. J., and Reynolds, J. M.: "Structure-from-Motion" photogrammetry: a low-cost, effective tool for geoscience applications, Geomorphology, 179, 300–314, 2012.
Westoby, M. J., Glasser, N. F., Brasington, J., Hambrey, M. J., Quincey, D. J., and Reynolds, J. M.: Modelling outburst floods from moraine-dammed glacial lakes, Earth-Sci. Rev., 134, 137–159, doi:10.1016/j.earscirev.2014.03.009, 2014.
Wohl, E. E.: Uncertainty in flood estimates associated with roughness coefficient, J. Hydraul. Eng., 124, 219–223, 1998.
Worni, R., Stoffel, M., Huggel, C., Volz, C., Casteller, A., and Luckman, B.: Analysis and dynamic modelling of a moraine failure and glacier lake outburst flood at Ventisquero Negro, Patagonian Andes (Argentina), J. Hydrol.,444–445, 134–145, doi:10.1016/j.jhydrol.2012.04.013, 2012.
Xin, W., Shlyln, L., Wanqin, G., and Junll, X.: Assessment and simulation of Glacier Lake Outburst Floods for Longbasaba and Pida Lakes, China, Mt. Res. Dev., 28, 310–317, 2008.
Yu, D. and Lane, S. N.: Urban fluvial flood modelling using a two-dimensional diffusion-wave treatment, part 2: development of a sub-grid-scale treatment, Hydrol. Process., 20, 1567–1583, 2006.
Zemp, M., Hoelzle, M., and Haeberli, W.: Six decades of glacier mass balance observations – a review of the worldwide monitoring network, Ann. Glaciol., 50, 101–111, 2009.
Zhang, S. and Duan, J. G.: 1D finite volume model of unsteady flow over mobile bed, J. Hydrol., 405, 57–68, 2011.

ESURFD
2, 477–533, 2014

Table 1. Parameter ranges and geometric characteristics of the Dig Tsho moraine dam used for input to the HR BREACH numerical dam-breach model. Input parameter ranges were established from a combination of initial experimentation and parameter sensitivity analysis (E), in situ field observation (F) and data from similar sites stated in the literature (L). All dam geometry data were extracted from the SfM-DTMs of the moraine and floodplain (SfM-DTM), with the exception of downstream Manning's n, which reflects a sedimentological valley floor characterisation of gravels, cobbles and rare large boulders (after Chow, 1959).

Input parameter/geometric characteristic	Range/value	Source (E/F/L)
Parameter		
Sediment flow factor	0.8–1.2	E
Erosion width : depth ratio	0.5–2	E
D50 (mm)	28–200	F; L (Worni et al., 2012; Xin et al., 2004)
Porosity (% voids)	0.01–0.3	E
Density (kN m^{-3})	19–24	E
Manning's n (m$^{-1/3}$ s)	0.02–0.05	F; L
Internal angle of friction (°)	25–42	E; L (Lebourg et al., 2004)
Cohesion (kN m^{-2})	0–100	E
Dam geometry		
Crest level (m OD)	4356	SfM-DTM
Foundation level (m OD)	4316	
Crest length (m)	250	
Crest width (m)	30	
Distal face slope (1 : x)	3.1	
Proximal face slope (1 : x)	15.2	
Downstream valley slope (1 : x)	0.19	
Downstream Manning's n	0.04	L (Chow, 1959)

ESURFD
2, 477–533, 2014

Table 2. Scenario-specific behavioural simulation count for individual likelihood measures. Note: all simulations deemed to be behavioural after application of LH1 (final breach depth) were retained for conditioning on LH2 (breach thalweg elevation profile.

	LH1, LH2	LH3
DT_control	76	7
DT_overtop_min	98	33
DT_overtop_mid	93	33
DT_overtop_max	91	29
DT_instant_1	90	49
DT_instant_3	55	17
DT_instant_5	20	2

ESURFD
2, 477–533, 2014

Table 3. Total percentile hydrograph outflow volumes for individual scenarios and following clustering.

	Total percentile hydrograph volume ($\times 10^6$ m^3)								
	LH1			LH1 + 2			LH1 + 2 + 3		
Scenario/Cluster	5th	50th	95th	5th	50th	95th	5th	50th	95th
DT_control	2.2	6.6	13.1	2.2	6.6	13.3	4.8	7.0	9.5
DT_overtop_min	1.8	6.5	14.4	1.7	6.5	14.2	1.2	6.6	15.2
DT_overtop_mid	1.5	6.4	15.0	1.5	6.2	14.6	1.3	6.3	16.0
DT_overtop_max	1.9	6.5	14.2	1.8	6.5	13.8	1.7	6.0	14.1
DT_instant_1	1.0	6.4	15.2	1.1	6.5	14.6	1.8	6.9	13.4
DT_instant_3	3.2	6.9	11.8	3.4	6.8	11.3	3.6	6.8	11.1
DT_instant_5	4.4	7.1	10.2	3.6	6.9	10.2	5.7	7.3	8.8
Cluster 1	2.1	6.6	13.8	2.4	6.8	12.9	1.6	4.4	8.8
Cluster 2	3.2	6.8	11.5	3.2	6.8	11.6	2.5	6.9	12.1
Cluster 3	3.2	6.8	11.2	3.1	6.8	11.5	3.0	6.7	11.6

ESURFD
2, 477–533, 2014

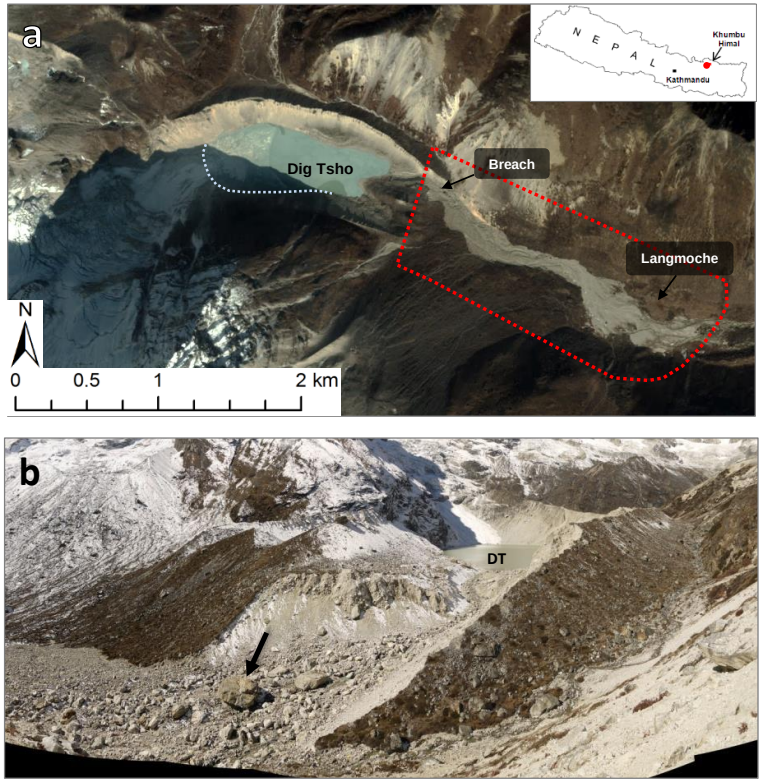

Figure 1. The Dig Tsho moraine dam and upper reaches of the Langmoche Khola. **(a)** True colour GeoEye imagery of the study site. Extensive reworking of the valley-floor by escaping floodwaters is evident immediately downstream of the moraine breach. Red dashes indicate two-dimensional model domain. **(b)** The moraine-dam breach, formed by the 1985 GLOF. For scale, the boulder indicated by the black arrow is > 10 m in height and diameter. The breach is ~ 200 m at its widest point, and has a maximum depth of 60 m. The relict Dig Tsho glacial lake is visible in the background (DT).

ESURFD
2, 477–533, 2014

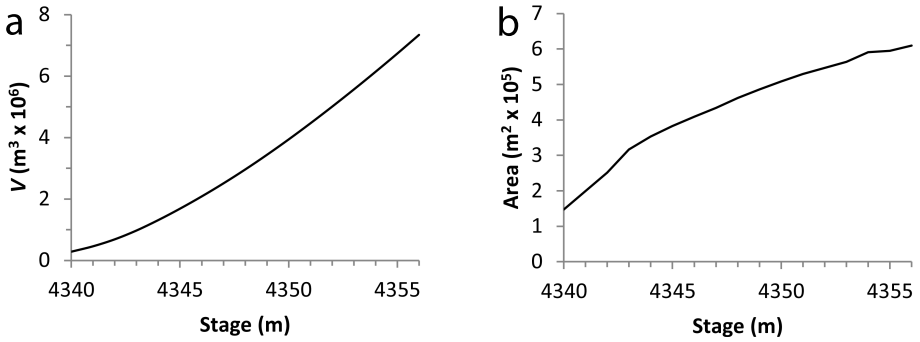

Figure 2. Bathymetric data describing **(a)** volume-stage, and; **(b)** area-stage relationships, extracted from a fine-resolution, Structure-from-Motion-derived digital terrain model of the Dig Tsho moraine-dammed lake basin (Westoby et al., 2012).

ESURFD
2, 477–533, 2014

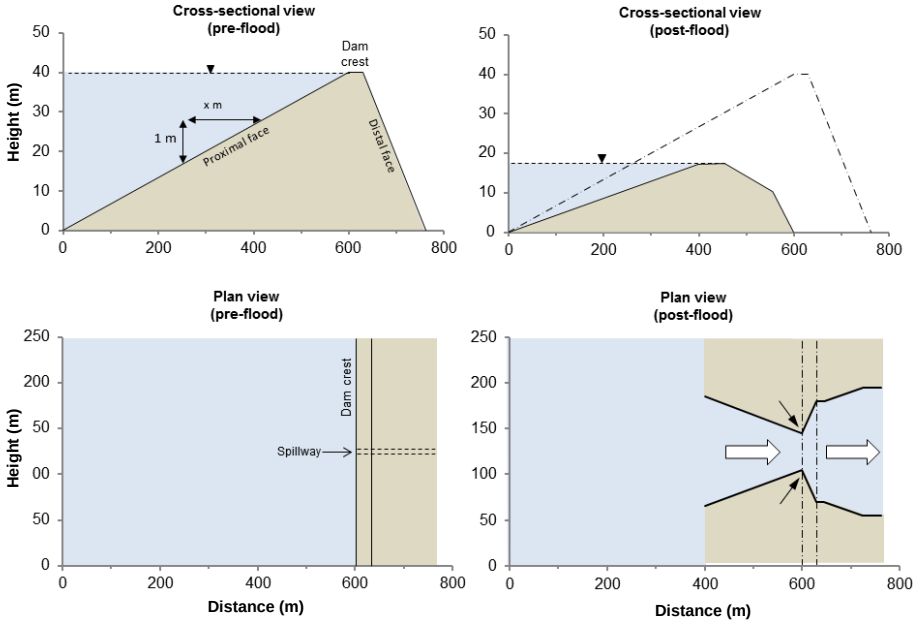

Figure 3. Schematic diagrams of initial (pre-flood) and an example of post-flood geometry for the Dig Tsho moraine dam (left and right columns, respectively), as modelled by HR BREACH. Initial dam face slope angle is represented as a ratio of the form $1 : x$. White arrows indicate flow direction. Solid black arrows (post-flood, plan view panel) highlight location of the critical flow constriction and used as a likelihood measure for model evaluation. Note vertical exaggeration of dam elevation.

ESURFD
2, 477–533, 2014

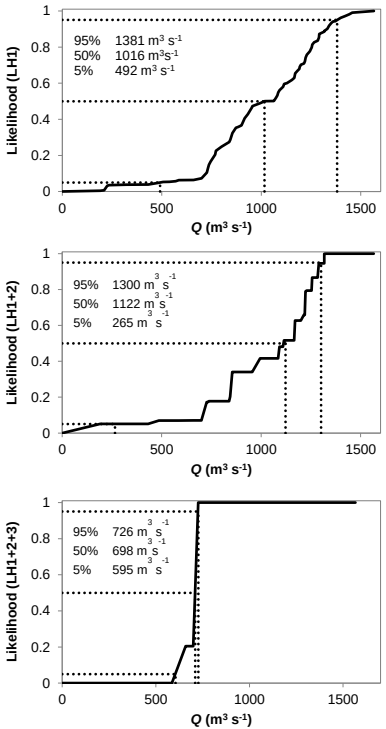

Figure 4. *DT_control* Cumulative Density Function (CDF) data for T = 150 min (solid line). Changes to likelihood values resulting from Bayesian updating are ultimately translated to changes in the form of the CDF curve, from which percentile Q data are extracted at 5, 50 and 95 % confidence intervals (dashes). LH1 = final breach depth; LH1 + 2 = final breach depth + centreline elevation profile; LH1 + 2 + 3 = final breach depth + centreline elevation profile + flow constriction location.

ESURFD
2, 477–533, 2014

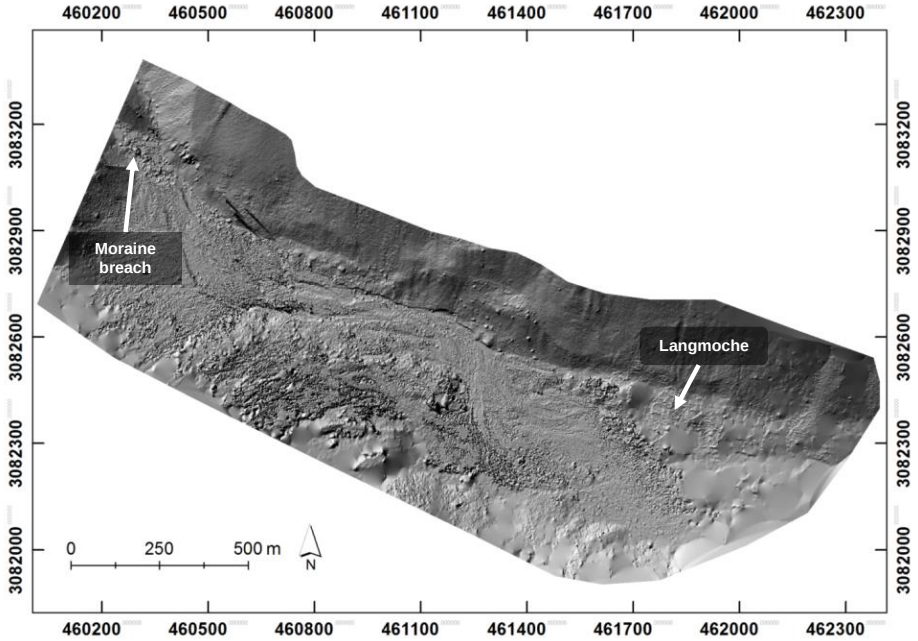

Figure 5. Hillshaded DTM of the Langmoche Valley floor (0–2.2 km from breach), produced using terrestrial photography from the valley flanks in combination with Structure-from-Motion photogrammetric processing techniques. Elevation data were extracted at 1 m^2 grid resolution (from detrended mean cell elevation) from the geo-referenced data (UTM Zone 45N). DTMs of the breached moraine-dam complex are displayed in Westoby et al. (2012). Individual boulders up to ~ 5 m in diameter are resolved. Areas of weak reconstruction to the south-east of the domain are attributed to poor photographic density and topographic obscurement.

ESURFD
2, 477–533, 2014

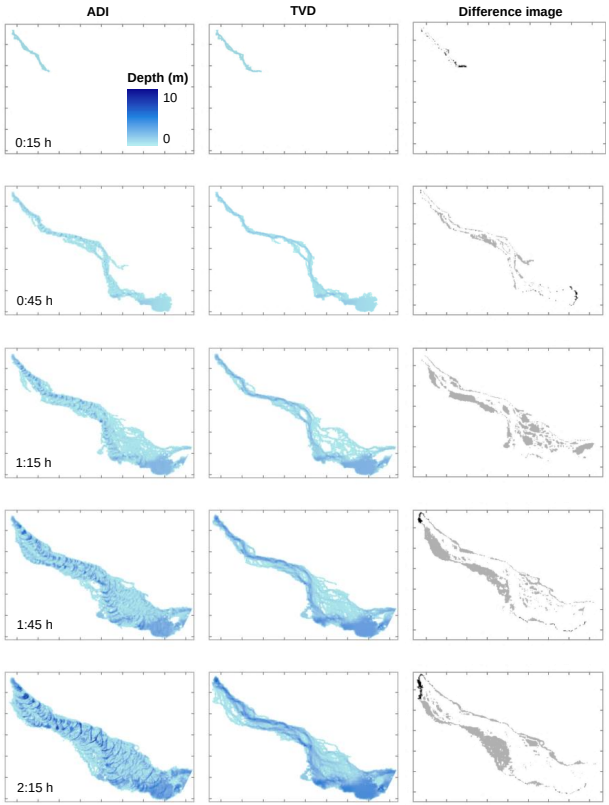

Figure 6. Comparison of GLOF inundation in the upper reaches of the Langmoche Khola using the ISIS 2-D Alternating Implicit Direction (ADI) and Total Variation Diminishing (TVD) solvers at selected time steps. Also shown is a difference image of inundation, where black and grey shading corresponds to areas inundated exclusively by the TVD and ADI solvers, respectively. See Fig. 1a for location. Inset tick marks spaced at 200 m intervals.

ESURFD
2, 477–533, 2014

Numerical modelling of Glacial Lake Outburst Floods

M. J. Westoby et al.

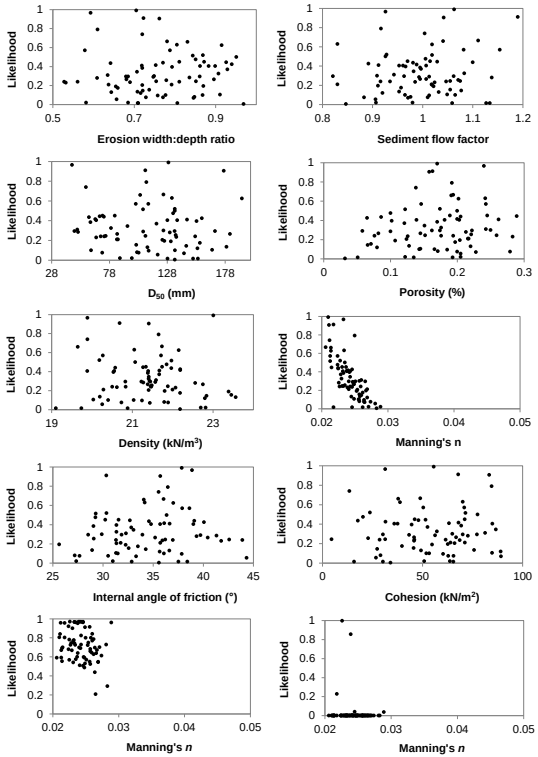

Figure 7. Scatter, or "dotty" plots, of likelihood values for HR BREACH input parameters for behavioural Monte Carlo simulations of *DT_control*, conditioned on final breach depth. Bottom two plots represent the Manning's *n* likelihood surface for results conditioned on final breach depth and residual slope error (left), and final breach depth, residual centreline elevation error and final flow constriction location (right).

ESURFD
2, 477–533, 2014

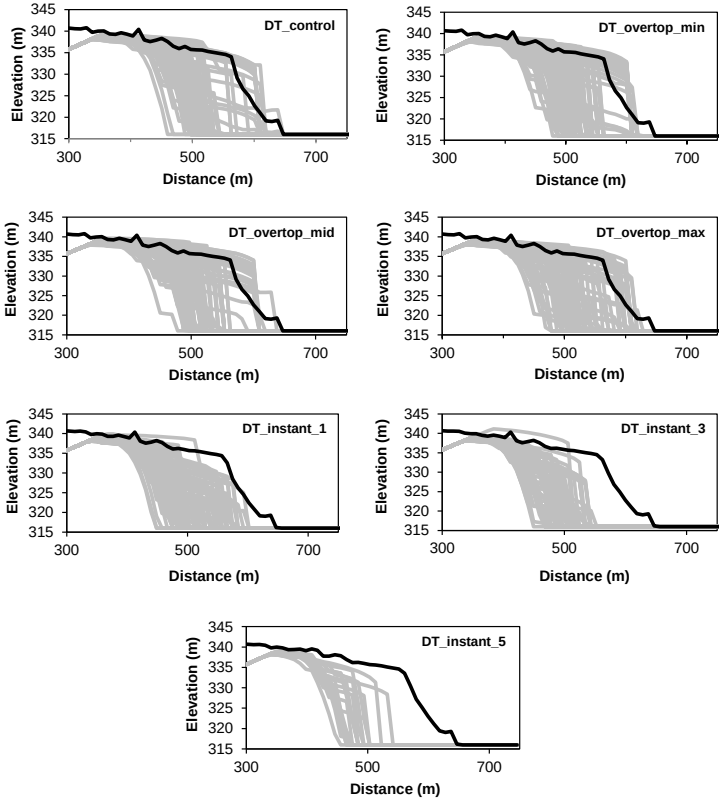

Figure 8. Final centreline breach elevation profiles for the Dig Tsho simulations. Black = observed profile; grey = modelled (behavioural) profiles.

ESURFD
2, 477–533, 2014

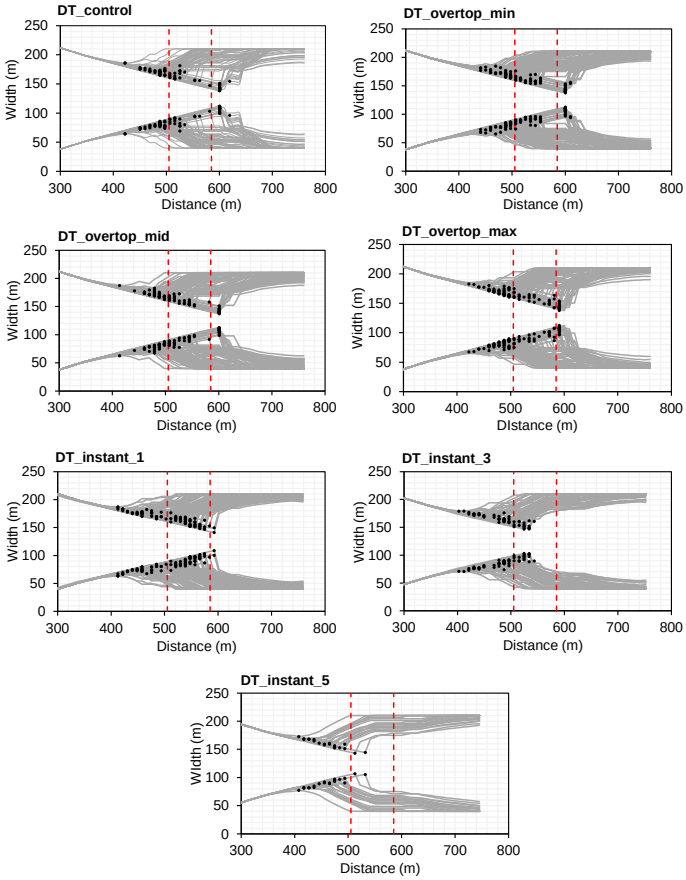

Figure 9. Final breach planforms (grey lines) for all modelled scenarios. Precise locations of critical flow constriction are highlighted by black dots. Simulations possessing flow constriction locations that fell between the red dashed lines (distance 505–585 m) were deemed to be behavioural and assigned positive likelihood values.

ESURFD
2, 477–533, 2014

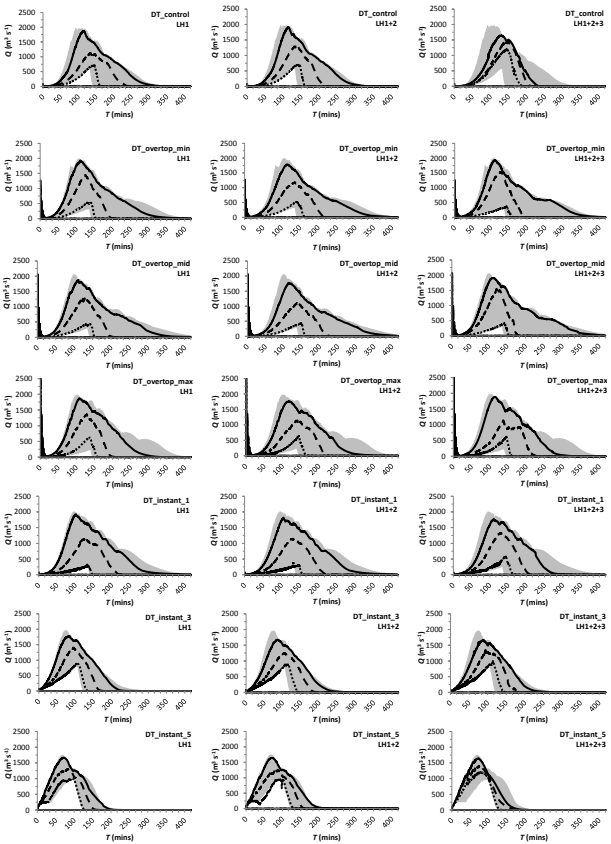

Figure 10. Percentile hydrographs derived from behavioural Dig Tsho simulations, for successive likelihood updating steps ("LH1", "LH1 + 2", "LH1 + 2 + 3"). 5th percentile = small dashes; 50th (median) percentile = long dashes; 95th percentile = solid black. Behavioural hydrograph envelope is displayed in grey.

ESURFD
2, 477–533, 2014

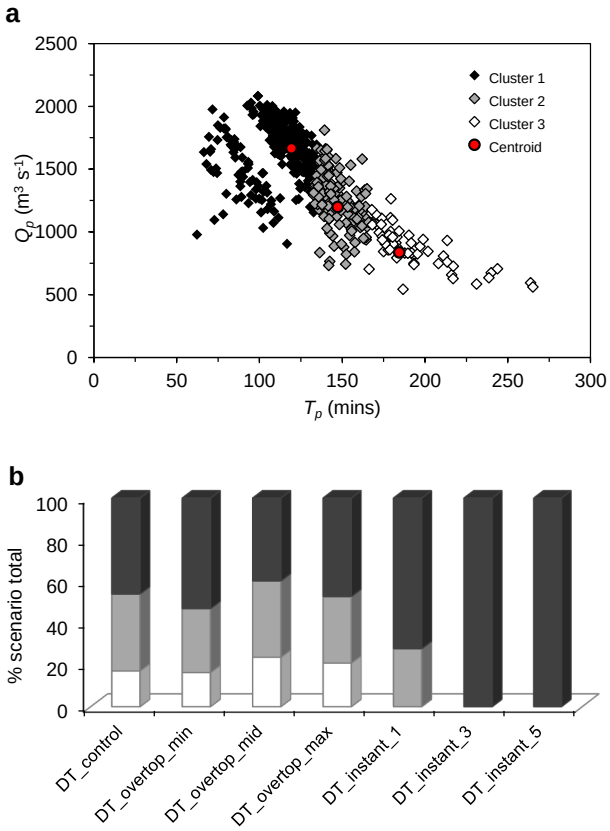

Figure 11. Data clustering. **(a)** Cluster membership following application of a subtractive clustering algorithm in MATLAB®; **(b)** Cluster membership as a function of total scenario-specific behavioural simulations (%). For key see **(a)**.

ESURFD
2, 477–533, 2014

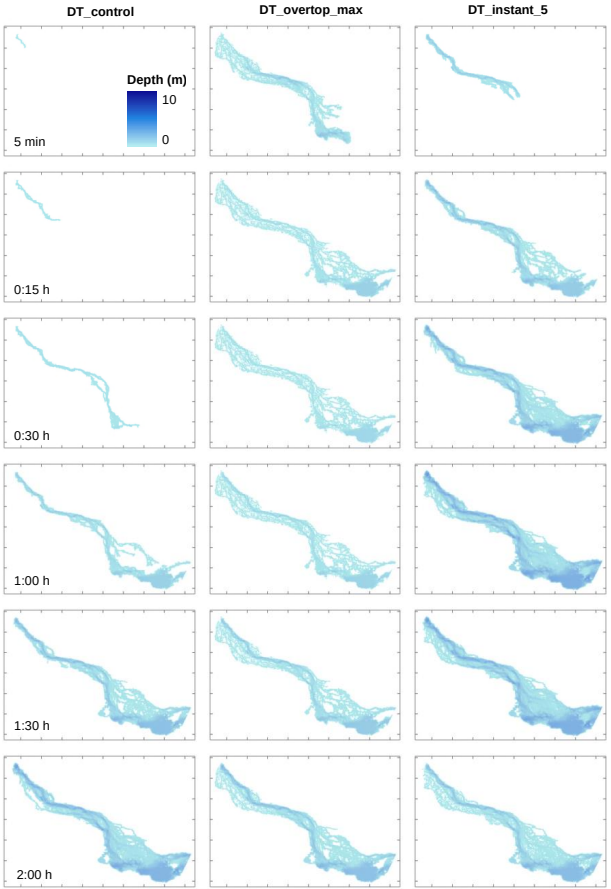

Figure 12. Inundation extent and flow depth distribution for selected time-steps for the *DT_control*, *DT_overtop_max* and *DT_instant_5* optimal flood even. See Fig. 1a for location. Inset tick marks spaced at 200 m intervals.

ESURFD
2, 477–533, 2014

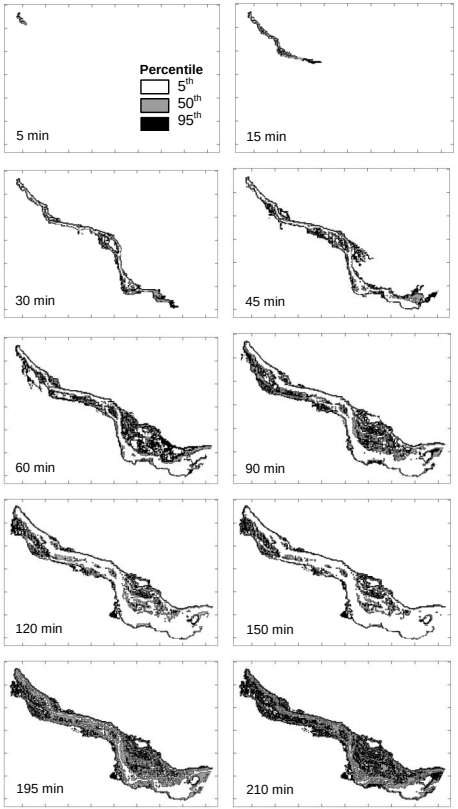

Figure 13. GLUE-based percentile maps of inundation for *DT_control*. 5th, 50th and 95th percentiles maps of inundation represent the water depth that would be exceeded with 95 %, 50 % and 5 % probability, respectively. See Fig. 1a for location. Inset tick marks spaced at 200 m intervals.

ESURFD
2, 477–533, 2014

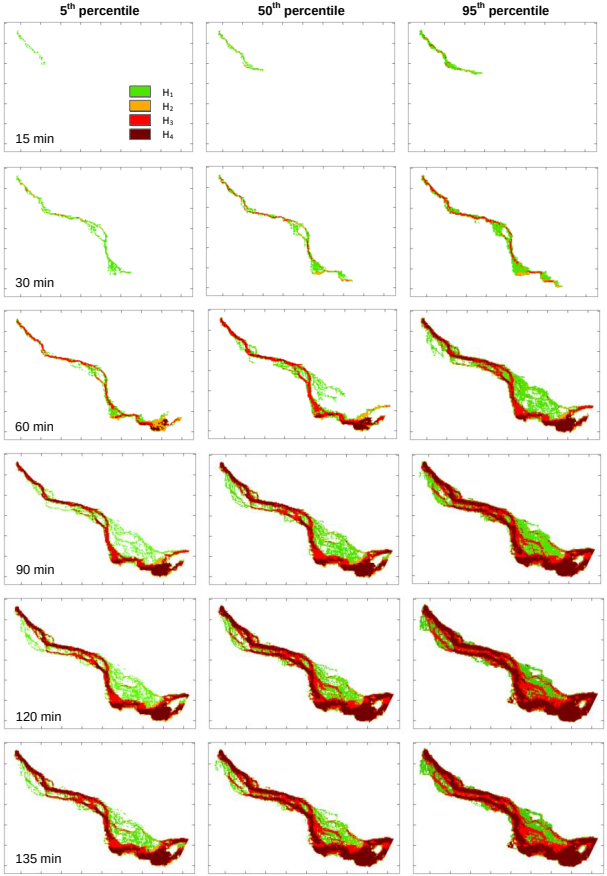

Figure 14. Percentile flood-hazard maps, based on a global hazard index forwarded by Aronica et al. (2012). Such data facilitate a probabilistic evaluation of the evolution of GLOF flood hazard. See Fig. 1a (this paper) for location, and Fig. 1b in Aronica et al. (2012) for description of the hazard index.

ESURFD
2, 477–533, 2014

Numerical modelling of Glacial Lake Outburst Floods

M. J. Westoby et al.

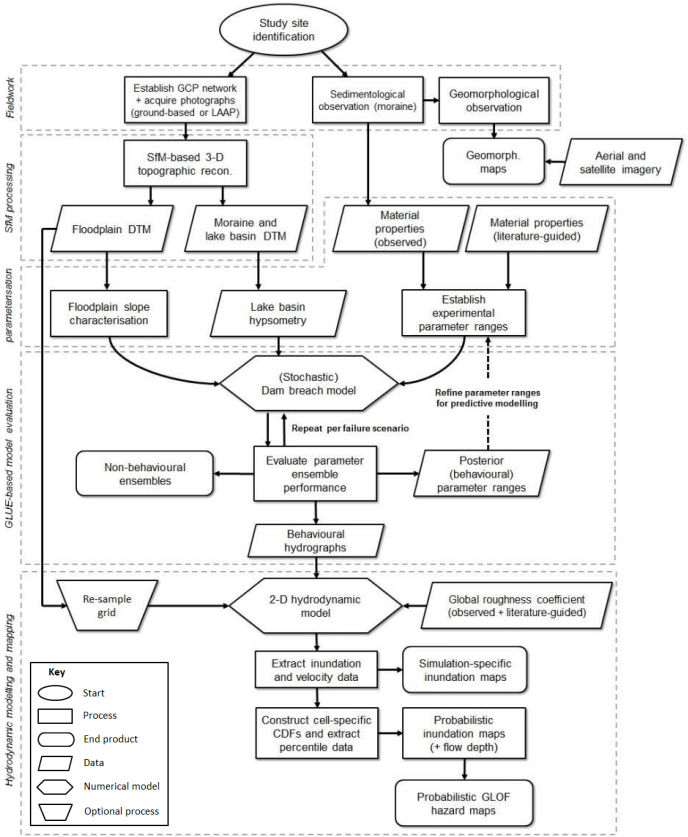

Figure 15. A unifying, "end-to-end" framework for probabilistic GLOF reconstruction incorporating high-resolution photogrammetry and probabilistic, GLUE-based numerical dam-breach and hydrodynamic modelling approaches.

ESURFD
2, 477–533, 2014